STANFORD GEOTHERMAL PROGRAM

QUARTERLY REPORT

OCTOBER 1 – DECEMBER 31, 1996

1 AN EXPERIMENTAL STUDY OF BOILING IN POROUS MEDIA

This research project is being conducted by Dr. Cengiz Satik. The objective of this study is to improve our understanding of the process of boiling in porous media by using both experimental and numerical methods.

1.1 SUMMARY

The objective of this work is to improve the understanding of the process of boiling in porous media. The ultimate goal is to obtain the two important but currently unknown functions of relative permeability and capillary pressure functions. One horizontal and one vertical experiment were conducted using Berea sandstone core samples. Difficulties were encountered in analyzing the results of the first preliminary boiling experiment: namely the apparent existence of a steam phase at inappropriately low temperatures. These results suggested several improvements to the design of the experimental apparatus. Upon the completion of these modifications, further horizontal and vertical experiments were conducted. Three-dimensional porosity and steam saturation distributions were determined using an X-ray CT scanner. The maximum difference between the centerline and wall temperatures for the horizontal experiment was found to be less than 2 ^{o}C, therefore, wall measurements were shown to be adequate to represent the temperature of a circular slice along the core. The steam saturation distributions calculated from the X-ray CT data did not show a significant steam override in any of the experiments. Steady-state steam saturation data showed a progressive boiling process with the formation of the three regions of steam, two-phase and liquid as the heat flux was increased. The previous problem of steam existing at inappropriate temperatures was not observed in the later vertical experiment. A comparison of the three-dimensional saturation profiles from both experiments showed a longer two-phase zone in the horizontal boiling case than that in the vertical case.

1.2 INTRODUCTION

The process of boiling in porous media is of significance in geothermal systems as well as in many other applications such as porous heat pipes, drying and nuclear waste disposal. Despite its importance in these applications, the fundamentals of this process are poorly understood. Most of the problems arise from the lack of the understanding of the mechanics and dynamics of this complex process.

A look at the previous literature shows that many attempts have been made in both experimental and theoretical directions to investigate and to describe the process of boiling in porous media (Satik, 1994). Most previous studies have used continuum formulations which made use of Darcy's law extended to multiphase flow with relative permeability and capillary pressure functions derived from isothermal gas-liquid displacement processes. These processes have major differences to boiling displacement which involves additional phenomena such as heat transfer, nucleation and phase change. Moreover, the continuum approaches are also limited by the assumption of capillary control at the pore level (low

Capillary and Bond numbers). Due to these restrictions and uncertainties, it is unclear whether the relative permeability and capillary pressure functions currently used for modeling the process of boiling in porous media are appropriate.

At the same time, fundamental studies focusing at the microscopic pore scale have been very limited. In a recent study by Satik and Yortsos (1996), numerical and experimental pore networks were used to model boiling in porous media at a microscopic pore scale. Satik and Yortsos (1996) developed a numerical pore network model for boiling in a horizontal, two-dimensional porous medium and conducted visualization experiments by using glass micromodels. Although progress was made, their model was developed only for a single bubble growth problem in a horizontal porous medium, ignoring the effects of gravity. Therefore, further work is still needed to improve the understanding and to resolve the issues raised by the continuum formulations (see Satik, 1994, for details) and eventually to obtain correct forms of the relative permeability and capillary pressure functions.

In this work, we used a different technique to study this problem. We conducted boiling experiments with real core samples such as from Berea sandstone. Using an X-ray computer tomography (CT) scanner, we visualized the process and determined the three-dimensional fluid distributions within the core while the experiment was in progress. By using thermocouples, pressure transducers and heat flux sensors under the control of a data-acquisition system, we obtained temperature, pressure and heat flux values along a core, respectively. The comparison of the experimental data with the results of a numerical simulator will give us an opportunity to check the results Moreover, using an optimization tool along with a numerical simulator combined with experimental results, the appropriate form of the relative permeability and capillary pressure functions can be obtained. Our ultimate goal is to be able to carry out these experiments with core samples taken from The Geysers geothermal field in California. Concurrent efforts are being directed towards the construction of an apparatus that can be used to carry out boiling experiments with low permeability core samples.

This paper reports on the results of two experiments conducted using Berea sandstone core samples. The core was positioned horizontally in the first experiment while it was vertical in the second one. Two complete sets of experimental data were collected. These will be discussed in detail here. The paper is organized as follows: We first describe the experimental apparatus, discuss the procedure followed and finally present the results of the two experiments.

1.3 EXPERIMENTAL APPARATUS AND PROCEDURE

A schematic of the experimental apparatus is shown in Figure 1.1. The apparatus consists of a core holder, a data acquisition system, a vacuum pump, a liquid pump and a balance. Ten pressure taps and thermocouples are placed along the core length to measure

pressures and temperatures, respectively. A heater and a heat flux sensor are placed in the specially designed inlet end of the core holder. In addition, several heat flux sensors are placed along the core to measure heat losses. During an experiment, the core holder is placed inside the high resolution X-ray CT equipment to obtain *in-situ* saturation profiles along the core. During CT scanning, an X-ray source is revolved around the object to take various projections at many angles and the data collected are then used to reconstruct the internal image. The method causes an averaging of X-ray attenuation as X-ray beams travel through the object while changes in density and/or thickness of the material cause differences in X-ray attenuation (Johns *et al.*, 1993).

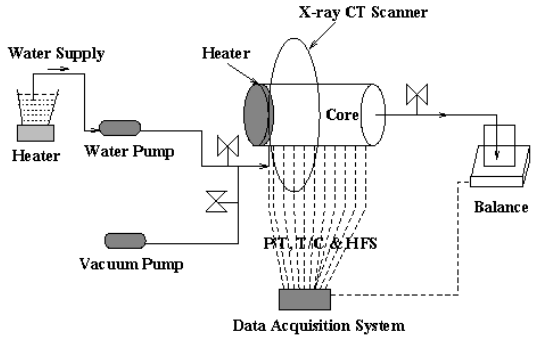

Figure 1.1: Schematic of the experimental apparatus.

The experimental procedure is as follows. First, air inside the pore space is removed by vacuuming the core. The core is then scanned at predetermined locations to obtain dry-core CT ($\mathbf{CT_{dry}}$) values. Next, deaerated water is injected into the core. This step continues until the core is completely saturated with water, at which time the core is X-ray scanned again at the same locations to obtain wet-core CT ($\mathbf{CT_{wet}}$) values. Also, pressure readings are taken at this time to calculate the absolute permeability of the core. Steady-state boiling experiments mainly involve the injection of heat into the core at varying power levels. During the experiment, the heating end of the core is closed to fluid flow while the other end is connected to a water reservoir placed on a balance. The balance is used to monitor the amount of water coming out of the core during the process. The core holder is covered with a 4 inch thick layer of insulation material to reduce the heat losses. In addition, several heat flux sensors are placed along the core to measure the actual heat losses. Continuous measurements of pressure, temperature and heat flux are taken during each heat injection rate step until steady state conditions are reached. During the boiling process each step continues until the water production rate becomes zero, and the pressures, temperatures and heat fluxes stabilize; these are indications of steady-state conditions. At the onset of steady-state conditions, the core is scanned again at the same locations to obtain CT ($\mathbf{CT_{exp}}$) values corresponding to the particular heat flux value. To complete the set of measurements, pressure, temperature and heat flux readings are recorded again. The heat flux is then changed, and the full procedure is repeated. After the experiment is completed, the porosity and saturation distributions are calculated from the **CT** values. More complete details of the calculation method were given in Satik *et al*. (1995).

The porosity distributions at various locations along the core are calculated by inserting $\mathbf{CT_{dry}}$ and $\mathbf{CT_{wet}}$ values into the following equation:

$$\phi = \frac{\mathbf{CT_{wet}} - \mathbf{CT_{dry}}}{\mathbf{CT_{water}} - \mathbf{CT_{air}}} \quad \textbf{(1.1)}$$

where $\mathbf{CT_{water}}$ and $\mathbf{CT_{air}}$ are CT numbers for water and air respectively.

Steam saturation distributions are also calculated by using the following equation:

$$\mathbf{S_{steam}} = \frac{\mathbf{CT_{wet}} - \mathbf{CT_{exp}}}{\mathbf{CT_{wet}} - \mathbf{CT_{dry}}} \quad \textbf{(1.2)}$$

1.3 RESULTS

Two experiments were conducted using two different Berea sandstone core samples. The core sample was positioned horizontally in the first experiment while it was positioned vertically in the second experiment. Two complete sets of experimental data were obtained from these experiments for the case in which the heat flux was increased. These included porosity and saturation distributions determined using the X-ray CT data, and also pressure, temperature and heat flux readings. The results obtained from these two experiments are discussed below.

The length and diameter of the cores used in both experiments were 43 cm and 5.04 cm, respectively. Before being used in each experiment, both cores were scanned using the X-ray CT scanner at various locations to ensure that they were free of inhomogeneties. Both cores were found to have very similar X-ray CT images. By using the Darcy equation with the results of the wet-core step during each experiment, the absolute permeability of both cores was calculated to be around 500 md. During both experiments, we scanned a total of 42 slices along the core. Using Equation (**1.1**) and dry and wet X-ray CT data, a three-dimensional porosity profile of each core was constructed. All of those slices for each core indicated a fairly homogenous core. The porosity data were then averaged over each circular slice in order to obtain porosity profiles given in Figure 1.2. The figure shows a uniform porosity distribution for both cores. The minimum, maximum and average porosity values were calculated to be 0.196, 0.208 and 0.2012 for the first core and 0.1826, 0.1881 and 0.1865 for the second core, respectively.

Recently, we reported the preliminary results from an earlier horizontal boiling experiment (Satik and Horne (1996). Rather unusual temperature profiles were found in the experiment. Comparison of the steam saturation profiles obtained from the X-ray CT scanning with the corresponding temperature and pressure profiles indicated an inconsistency. The steam saturation profiles showed non-zero values up to temperatures of as low as 50 ^{o}C. Although pressures were not measured during this experiment they were assumed to be above atmospheric pressure since the outlet of the core was connected a water reservoir placed next to the core. This unusual behavior was initially attributed to air trapped inside porous medium and air dissolved in the water used to saturate the porous medium (Satik and Horne, 1996). To remedy this problem, the experimental procedure was changed to remove any possible preexisting gas phase in the system. During the new procedure, the core was first vacuumed to 0.00319 psi before the experiment. The water used to saturate the core was then deaerated by preboiling it in a container.

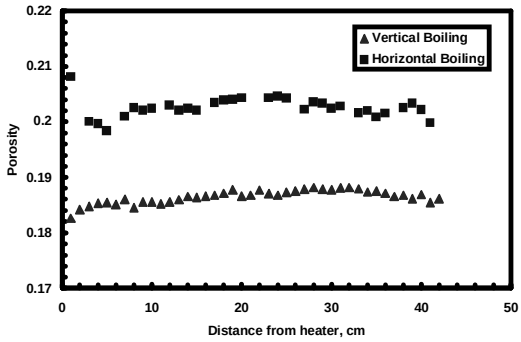

Figure 1.2: Average porosity profiles along the core, calculated from X-ray CT data obtained during both boiling experiments.

During the first experiment, in which the core was horizontal, the core was scanned and three-dimensional porosity distributions were obtained eight times before and after heating in order to observe the first formation of the steam phase. These three-dimensional porosity distributions were then averaged over each circular cross-section of the core that was scanned in order to obtain the average porosity profiles, four of which are given in Figure 1.3. All of the curves displayed in the figure, except the curve at 2770 min, show a fairly uniform porosity profile along the core and are within close proximity to each other. The deviation of the curve at 2770 min at distances closer to the heater suggests the first appearance of the steam phase. The comparison of all eight porosity curves with pressure and temperature data indicated that a steam phase did not appear until the appropriate boiling temperature. This results is important because it confirms that air was successfully removed from both porous medium and the water used to saturate it.

Both boiling experiments were conducted by increasing the heater power setting incrementally to reach a desired heat flux value. Figure 1.4 shows the history of the heater power settings and the heat flux values obtained from heat flux sensors for both horizontal and vertical experiments. The same heater was used in both experiments, thus the magnitude of the power generated by the heater was similar in both cases at the same power setting value.

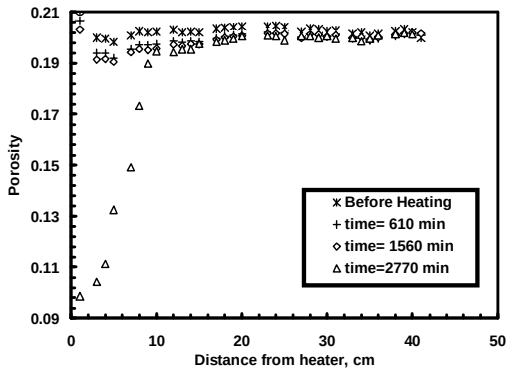

Figure 1.3: Average porosity profiles along the core, obtained from the X-ray CT scanning conducted at four times during the horizontal boiling experiment.

During the horizontal experiment, we recorded both the centerline and wall temperatures at ten locations along the core. The centerline temperatures were measured in thermowells extending to the center of the core. The wall temperatures were measured over the outer layer of the epoxy and next to the thermowells. In Figure 1.5, we show the comparison of the histories of the centerline and wall temperatures obtained at four locations along the core length. The figure shows both transient and steady state (where the temperature profile flattens) sections of the temperature profiles at each heater power value. The maximum temperature reached during the first experiment was 225^{o}C. As shown in Figure 1.5, the maximum difference between the two temperature profiles was less than 2^{o}C. This suggested that the radial temperature gradient along the core was not significant for this set of experimental conditions and therefore it would be adequate to measure wall temperatures only.

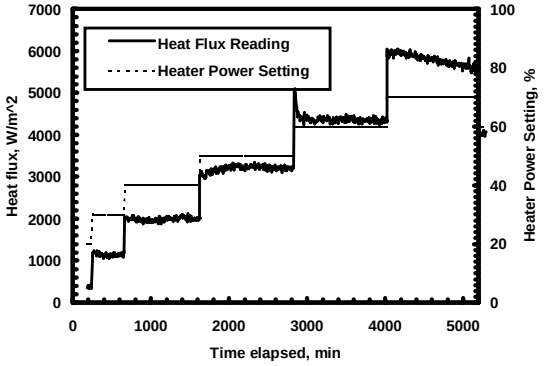

(a)

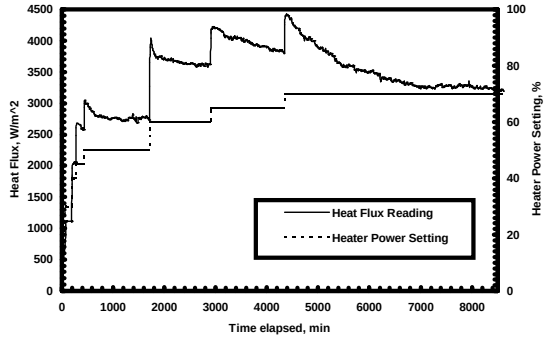

(b)

Figure 1.4: Heater power settings and corresponding heat flux values obtained from the heat flux sensor: (a) horizontal experiment, (b) vertical experiment

The core was scanned several times to obtain three-dimensional steam saturation distributions during the experiment. These three-dimensional steam saturation distributions were then averaged over each circular cross-section of the core that was scanned in order to obtain the average steam saturation profiles. In Figure 1.6, we show four of these saturation profiles. The saturation profile at 2770 min shows a two-phase (steam and water) zone followed by a completely water-filled zone while the profile at 5130 min shows three distinct regions of completely steam, two-phase and completely water. As expected, the steam saturation is higher at locations closer to the inlet, where the heater is located, and decreases towards the outlet.

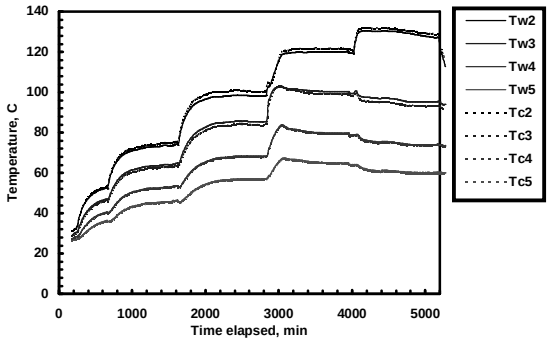

Figure 1.5: Comparison of the histories of four centerline and wall temperatures during the horizontal boiling experiment.

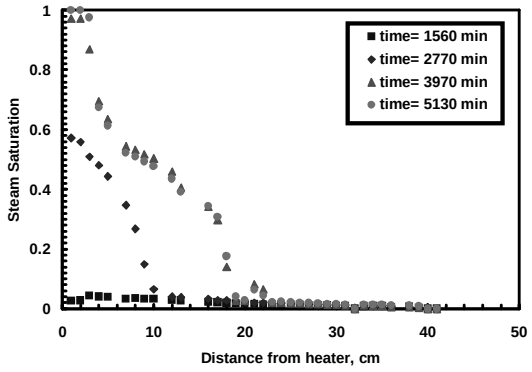

Figure 1.6: Average steam saturation profiles along the core, calculated from X-ray CT data during the horizontal experiment.

The comparison of the saturation profile with the corresponding centerline temperature profile at 5130 min is shown in Figure 1.7. Steam saturation at $100^{o}C$ is about 56% and vanishes at about $52^{o}C$. This suggests that the previous problem of the apparent existence of a steam phase at inappropriate temperatures still existed. This behavior was also observed on the other profiles obtained at different.

Following the horizontal experiment, another experiment was conducted with the core holder positioned vertically to study the effect of gravity on the results. Since the core used for the horizontal experiment had developed extensive cracks during the cooling stage, another core that had similar properties was prepared and used for the vertical experiment. This experiment was also carried out by varying the heater power setting from 20% to 70% incrementally (Figure 1.4b). Again, to ensure the removal of any gas phase existing in the porous medium or dissolved in the water saturating it, the procedure employed in the first experiment was also used in the vertical experiment.

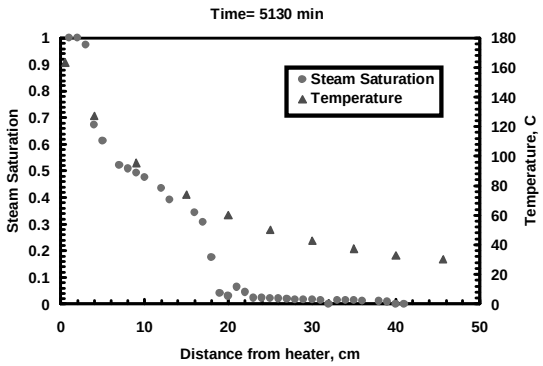

Figure 1.7: Comparison of the steam saturation and temperature profiles along the core during the horizontal boiling experiment.

Measurements of temperature and pressure were taken at ten locations along the core during the experiment. The temperature profiles in Figure 1.8a show the transient and stabilization stages of each power change. On the other hand, the pressure profiles seem to exhibit an oscillatory behavior until about 5500 min at which time they start to stabilize (Figure 1.8b). Although not recognizable due to the scale of the graph in Figure 1.8a, these oscillations also exist in the temperature profiles.

In Figure 1.9, we show pressure, temperature and saturation profiles obtained at four times during the vertical experiment. Each profile was obtained at the onset of steady-state conditions after each time the heater power was changed. At the beginning of the heating (the curves at 0.022 min), temperatures, pressures and steam saturations along the core was at room temperature, hydrostatic pressure and zero, respectively. After the heater power was increased to 50% (see also Figure 1.4b) temperatures close the heater started to raise (Figure 1.8a). The saturation profile at 1610 min shows about 60% steam saturation at the closest location to the heater. The corresponding pressure profile is consistent with the saturations, showing higher pressures closer to the heater that may also indicate the formation of steam phase. As the heater power was increased further, dry-out conditions occurred, leading to existence of the three zones of dry steam, two-phase and liquid water zones (profiles at 2795, 4230 and 8550 min). However, the pressure profiles at 4230 and 8550 min show an unusual behavior, a decrease at all locations along the core. Currently we do not understand the cause of this pressure drop but it could be attributed to a small leak in the core or to a complication with pressure transducers. The pressures increased again during the cooling stage of the experiment, indicating a possible problem with the pressure transducers. To improve the accuracy of pressure measurements in the experiments, the acquisition of more accurate pressure transducers is in progress.

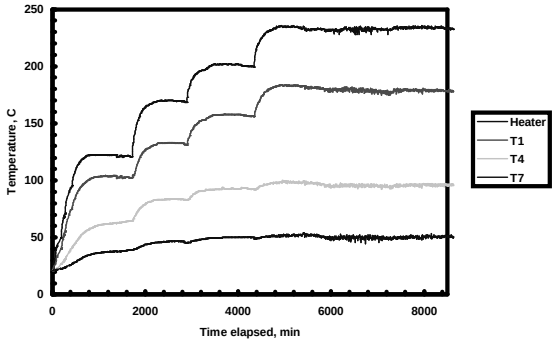

(a)

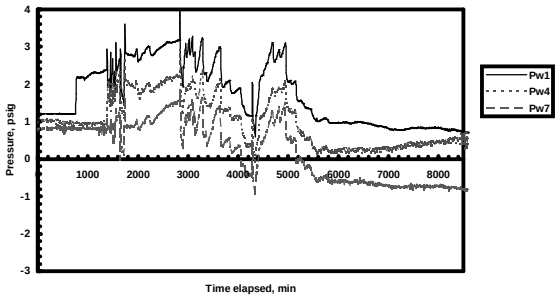

(b)

Figure 1.8: Histories of (a) temperature and (b) pressure obtained during the vertical boiling experiment.

The temperature profiles showed consistent behavior this time. The previous problem of steam phase existing at inappropriate temperatures did not exist in this experiment. As illustrated in Figure 1.10, the steam saturation profile indicates a dry steam zone and a liquid water zone connected by a two-phase region. Temperatures are consistent with saturations: A substantial temperature drop in the dry steam zone is due to the low steam-phase thermal conductivity, a rather small temperature gradient in the two-phase zone is due to the pressure gradient and heat losses and the temperature profile in liquid water zone.

In Figure 1.11, we show three-dimensional steam saturation profiles, obtained by X-ray CT scanning, at four times during the vertical experiment. The time values corresponding these four images are 1610, 2795, 4230, and 8550 min. The first image shows a two-phase zone followed by liquid water zone while the other three images have the three regions of steam, two-phase and liquid water. These images also show that the boundary between the dry steam and two-phase zone is sharp, indicating a uniform temperature distribution within the dry steam zone. The two-phase zone, on the other hand, has a different behavior. Within the two-phase zone, steam saturation is higher towards the edges of the

core while the water saturation is higher closer to the centerline of the core, indicating a possible two-phase convection.

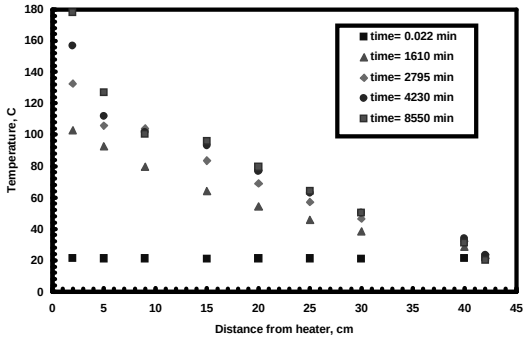

(a)

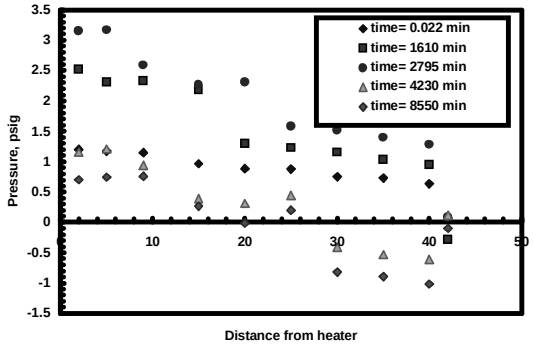

(b)

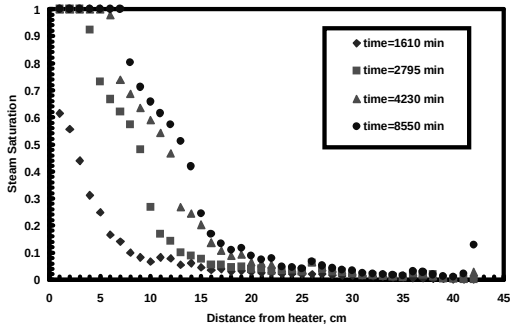

(c)

Figure 1.9: Steady state (a) pressure, (b) temperature and (c) steam saturation profiles along the core, obtained during the vertical boiling experiment.

Finally, in Figure 1.12 we show a comparison of the steam saturation profiles of both horizontal and vertical experiments at the same power values. These results show the effect of gravity. In the horizontal case, the length of the dry steam zone is shorter and the

two-phase zone is longer than those in the vertical case. These results are expected since the two-phase zone, which has large compressibility, is expected to shrink in the vertical case simply due to the gravity of the liquid layer overlaying it.

1.4 CONCLUDING REMARKS

Two boiling experiments were conducted by using Berea sandstone core samples: one with a horizontal core and another with a vertical core. In a previous paper (Satik and Horne, 1996), we reported on the results of the first preliminary horizontal boiling experiment during which we observed an inconsistency in the apparent existence of a steam phase at inappropriately low temperatures. Analysis of the results suggested several improvements on the design of the experimental apparatus and procedure (Satik and Horne, 1996). With the new apparatus and procedure, one horizontal and one vertical experiment were conducted. Using an X-ray CT scanner, three-dimensional porosity and steam saturation distributions were obtained during the experiments. Temperatures, pressures and heat fluxes were also measured. In the new experimental method, both the core and the water used to saturate it were deaerated before the experiments. Both centerline and wall temperatures were measured during the horizontal experiment. The maximum difference between the centerline and wall temperatures was found to be less than $2^{o}C$, hence the wall temperatures were found to be adequate to represent the temperature of a circular slice along the core. Steady-state steam saturation distributions showed a progressive boiling process with the formation of the three regions of steam, two-phase and liquid as the heat flux was increased. The steam saturation distributions obtained using the X-ray CT data did not indicate any significant steam override in either experiment. The previous problem of steam existing at inappropriate temperatures was not observed in the vertical experiment although it persisted to a small extent in the horizontal case. The cause of this effect is still undetermined. Comparison of the three-dimensional saturation profiles from both experiments indicated a longer two-phase zone in the horizontal case than that in the vertical case. This result is expected since the two-phase zone has higher compressibility. Pressure data obtained from both experiments indicated possible problems with pressure transducers. Improvements to the accuracy of the pressure measurements are currently in progress.

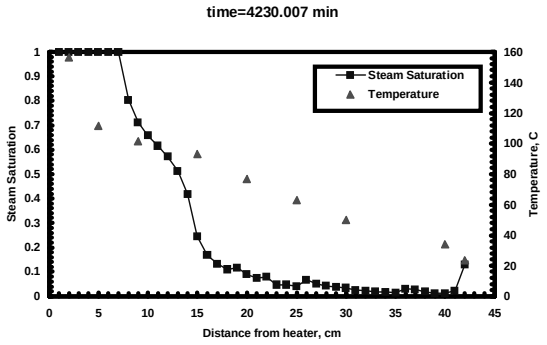

Figure 1.10: Comparison of the steam saturation and temperature profiles along the core during the vertical boiling experiment

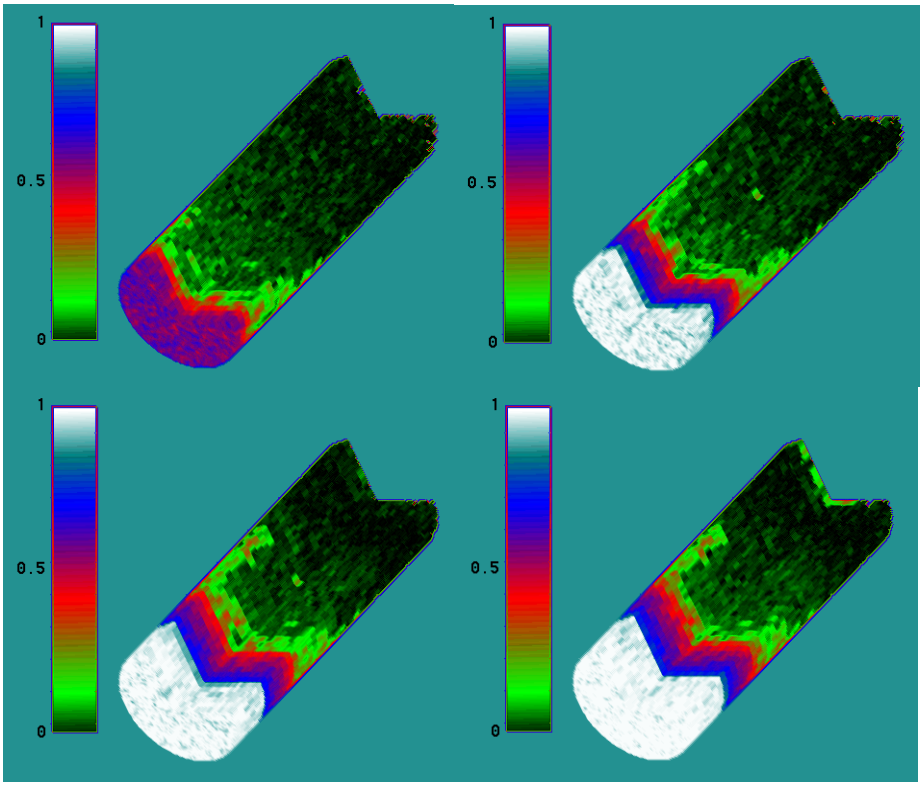

Figure 1.11: Three-dimensional steam saturation distributions along the core, calculated from the X-ray CT data obtained at four times during the vertical experiment.

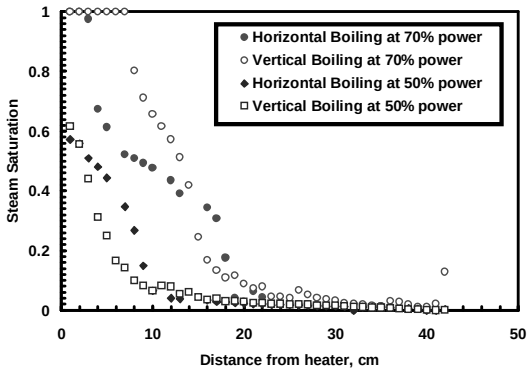

Figure 1.12: Comparison of the steam saturation profiles obtained at the same heater power values during the horizontal and vertical experiments.

2 INJECTION INTO GEOTHERMAL SYSTEMS

This work has been conducted by Program Manager Prof. Shaun D. Fitzgerald, Visiting Professor Andrew W. Woods and Undergraduate Research Assistant Catherine Tsui-Ling Wang. This quarter, we present the results of a suite of experiments which have been performed in order to determine the effects of injection into geothermal reservoirs. The results obtained from the experiments are compared with theoretical predictions of the evolution of temperature profiles within a geothermal reservoir following the injection of supercooled liquid. For the case of constant rate liquid injection in an axisymmetric geometry into a liquid-filled porous medium, we find that at slow rates of injection heat is conducted from the far-field towards the source. However, at higher rates of injection, an isothermal zone develops close to the injection well.

We conducted an experiment in which liquid was injected into a porous slab initially filled with superheated vapor. We compared the evolution of the temperature profile within the system with the theoretical prediction (Woods and Fitzgerald, 1997) and found that a sharp interface may develop between the liquid- andvapor-filled regions.

Finally, we investigated the injection of liquid into a fracture which initially contains superheated vapor. We compared the evolution of the temperature profile within the fracture with a numerical prediction obtained from TOUGH2 (Pruess, 1991). It was found that a broad two-phase region exists between the completely liquid-filled and vapor-filled zones of the system.

2.1 INTRODUCTION

As geothermal reservoirs are exploited for power production or district heating, they become depleted and reservoir pressures fall. As a result of the potential significant reduction in well flow rates, injection is now viewed as a strategic element of an exploitation program for a geothermal reservoir. The additional pressure support that is possible through the reinjection of spent brine can help minimize the reduction in pressure. However, although the potential benefits of additional pressure support by injection are large, there is a risk of breakthrough of cooler injected fluid at the production wells. If cold fluid reaches a production well the effects can be devastating. The specific enthalpy of the produced fluid falls. This leads to an increase in the average density of fluid within a production well, and therefore, the flowrate also decreases. The ability to predict the time at which injected cold fluid reaches a production feed zone is important and a number of modelling studies have been performed aimed at determining the evolution of the temperature profile within a reservoir following the onset of injection (Pruess *et al*., 1987; Woods and Fitzgerald, 1993, 1996, 1997).

In this report we present the results obtained from a series of analogue laboratory experiments which were performed to investigate liquid injection into geothermal

reservoirs. We first discuss the case of liquid injection into a liquid-filled porous medium and compare the experimental findings with the predictions obtained from a theoretical model (Woods and Fitzgerald, 1996). We then present the results obtained from an experiment in which liquid was injected into a porous medium initially filled with superheated vapor. The evolution of the temperature profile within the system is found to agree with the theoretical model proposed by Woods and Fitzgerald (1996). Finally, we consider the case of liquid injection into a fractured system. The experimental findings are compared with predictions obtained from a numerical model TOUGH2 that was modified to enable us to model the boiling of ether within the fracture.

2.2 LIQUID INJECTION INTO A LIQUID-FILLED POROUS MEDIUM

We have performed a series of experiments to test the model of liquid injection into a porous layer developed by Woods and Fitzgerald (1996). In the first suite of experiments, the apparatus consisted of a cylindrical bed of consolidated permeable sand, of radius 35cm and 3cm deep enclosed between two impermeable layers of epoxy resin. The sand bed consisted of 82% 30 mesh sand and 18% Portland cement. Twelve thermocouples were embedded into the sand layer at approximately 1cm radial intervals from the central injection port and these were connected to a digital data recorder. Before each experiment, carbon dioxide was injected into the center of the apparatus in order to displace the air. Cold de-ionized water was subsequently injected in order to displace the carbon dioxide. Any remaining CO_2 dissolved in the water. Insulating material was then placed on the upper and lower surfaces of the epoxy boundaries and the apparatus was connected to a water pump and heater.

In each experiment water was supplied at a constant rate, which was varied from experiment to experiment in the range 5-50 ml/min. For convenience, hot water was injected into a cold liquid-filled sand bed and several experiments were conducted using different flow rates and injection temperatures. The primary advantage of using a sand bed filled with liquid at room temperature, rather than at an elevated temperature, was that the risk of exsolution of any dissolved gases at room temperature was minimized. After completion of the experiments two CT scans of the sand layer apparatus were taken, one with the core fully dry and one with the core fully saturated with liquid. Using these measurements, the porosity ϕ was estimated to be 35+/-3%. Using this estimate together with the known properties of the sand, the effective thermal diffusivity of the porous medium was calculated to be 1.3+/-0.1E-06m^2/s. During each experiment, temperature measurements were recorded every 5s.

We wish to use the results obtained from these experiments in order to test the theoretical prediction proposed by Woods and Fitzgerald (1996). In this regard we developed a similarity type solution for the evolution of the temperature profile as a function of radius and time for the case in which liquid is injected at a constant rate $2\Pi Q$ from a central source in an axisymmetric geometry. Following the theory of Woods and Fitzgerald (1996, 1997), the temperature profile is expected to develop according to

$$T(\eta) = T_o + \Delta T \int_0^{\eta} \eta^{\lambda_w \beta - 1} \exp\left(-\eta^2\right) d\eta \qquad (2.1)$$

where $\beta = Q/\kappa$,

$$\Delta = \left(T_2 - T_0\right) / \int_0^{\infty} \eta^{\lambda_w \beta - 1} \exp\left(-\eta^2\right) d\eta \qquad (2.2)$$

T_0 is the source temperature, T_2 is the far-field temperature, $\lambda_w = \rho_l C_{pl} / (\phi \rho_l C_{pl} + (1-\phi)\, \rho_r C_{pr})$, ρ_l and ρ_r are the densities of liquid water and rock respectively, C_{pl} and C_{pr} are the specific heat capacities of liquid and rock, and κ is the average thermal diffusivity of the liquid-filled porous medium.

In Figure 2.1 we compare the temperature profiles obtained in an experiment with the theoretical predictions for the case $\beta=0.67$ and $\beta=3.4$. The radial locations of these measurements have been non-dimensionalized $\eta = r/(2\kappa t)^{1/2}$ and the temperature profiles are shown as a function of η. For both the fast injection case $\beta=3.4$ and the slower injection case $\beta=0.67$, the experimental results collapse accurately onto the theoretical temperature profiles.

The experimental data confirms the theoretical prediction that at low flow rates ($\beta < 1/\lambda_w$, Figure 2.1(i)), the isotherms are advected more slowly than the rate of conduction, so the internal boundary layer extends back to the source. However, at high flow rates ($\beta\lambda_w > 1$, Figure 2.1(ii)), the liquid is heated to the far-field temperature by cooling the rock near the source.

We now extend our discussion to investigate the case of liquid injection into a porous medium initially containing superheated vapor.

2.3 LIQUID INJECTION INTO A VAPOR-FILLED POROUS MEDIUM

Following the exploitation of a number of geothermal reservoirs such as The Geysers, there now exist zones in which the reservoir pressure is below the local saturation pressure corresponding to the reservoir temperature. These regions are prime candidates for the injection of liquid since it is in these regions that the pressure has usually declined most significantly, thereby leading to dramatic decreases in flow rate from the production well. In addition, the reduction in pressure and formation of reservoir superheat has created the possibility for injection of fluid and subsequent vaporization of this fluid. We now extend the experimental techniques developed in the previous section to the case in which an analogue reservoir initially contains superheated vapor.

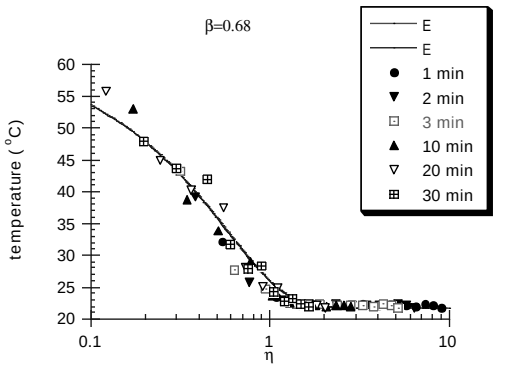

(i)

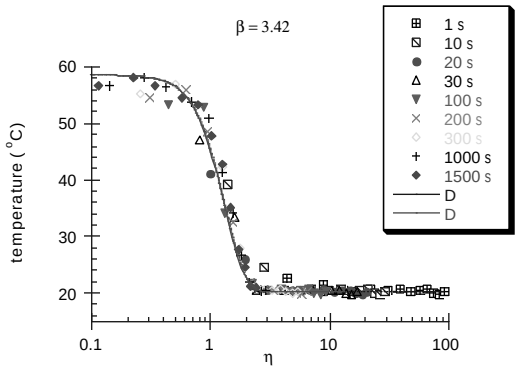

(ii)

Figure 2.1 Comparison of the model predictions with experimental measurements of temperature as a function of distance from the source. Distances are shown in dimensionless form $\eta = r/(2\kappa t)^{1/2}$*. Results are shown for two experiments in which hot liquid is injected into a cold water saturated layer. (i)* $\beta = 0.67$*, T(input)=63 C and T(initial)=20.2 C and (ii)* $\beta = 3.42$*, T(input)=59 C and T(initial)=21 C. Symbols show the temperature at different times during the experiment. The solid lines correspond to the theoretical prediction.*

The apparatus used in these experiments consisted of a slab of 500 md, 15.5% porosity Berea sandstone, 12in in diameter and 0.95in thickness. The sandstone core was initially heated in an oven to 500°F for 24 hours in order to deactivate the clays. This was performed in order that during the injection experiments, the clays did not swell and thereby block the pores. 12 thermocouples were then placed at various distances from the center of the disk and a central injection port was also drilled. The thermocouple holes were aligned along three radial transects and were drilled to a depth of 0.475in so that the thermocouples recorded the temperatures at the center of the slab. Epoxy resin was applied to the upper and lower surfaces of the sandstone core to form impermeable boundaries and the core was then flooded with carbon dioxide.

In order to study the boiling of liquid within the porous medium, the apparatus was heated in a oven at 108^{o}C for several hours. The apparatus was then removed from the oven, laid horizontally on insulating material and covered with additional pieces of insulation. Deionized water which had been heated to approximately 75^{o}C was then pumped through the injection port at a rate of 10ml/min. Temperatures were recorded every 5s by a digital data recorder.

Woods and Fitzgerald (1996, 1997) presented a theoretical model for the evolution of the system as liquid is injected at a constant rate into a porous medium in an axisymmetric geometry. In this model, the temperature profile is also described by a similarity solution in terms of the variable $\eta = r/(2\kappa t)^{1/2}$. The theoretical prediction obtained from Woods and Fitzgerald (1996, 1997) is plotted in Figure 2.2 with the experimental data.

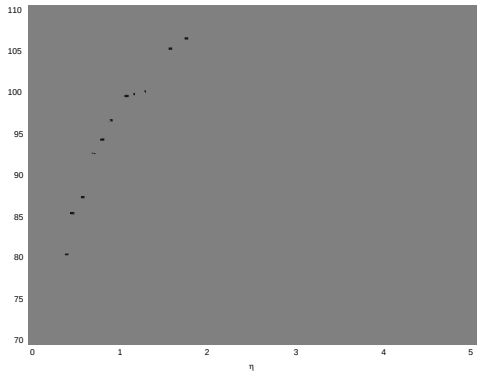

Figure 2.2 Temperature as a function of η *for an experiment in which water was injected at 73^{o}C into a sandstone core initially at 108^{o}C. The injection rate of 10ml/min into a core 0.95in thick corresponded to the case* $\beta = 0.67$*. Symbols represent the experimental data and the solid line indicates the theoretical prediction. Each set of symbols corresponds to temperatures obtained from one thermocouple.*

The temperature profiles within both the liquid- and vapor-filled regions are in close agreement with those predicted from the theory. Furthermore, the interface between the liquid- and vapor-filled zones is found to be sharp, in accord with the theoretical model. However, there are some noticeable discrepancies. In particular, the experimental data indicates that the temperature does not necessarily increase monotonically with radius away from the injection port. 12 thermocouples were used in the experiment, 4 thermocouples aligned along 3 different radial segments. The variation in temperature along each line of 4 thermocouples indicated that the boiling interface did not propagate as a circular front. If the apparatus was not perfectly level, then a non-circular front would be expected. However, we are reasonably confident that the apparatus was level. Propagating boiling fronts can become unstable if the fraction F which boils is sufficiently high (Fitzgerald and Woods, 1994).

However, in the present experiment the fraction which boiled was approximately 7% which is much less than the critical value. As a result, it is likely that the departures in temperature away from the theoretical prediction were caused by heterogeneities in the permeability of the sandstone core. Even though the scatter in the data indicates that the interface did not propagate uniformly, the general agreement between the experimental data and the theory suggests that the theory is valid over length scales greater than the scale of non-uniformity of the front.

The close agreement between the experimental data and model predictions for injection into porous media is comforting. However, geothermal reservoirs can also contain extensive zones of fractured rock. We have therefore extended our study of liquid injection into superheated rock to investigate the effects of injection into an isolated fracture.

2.4 LIQUID INJECTION INTO A VAPOR-FILLED FRACTURE

In the case of liquid injection into a porous medium filled with superheated vapor, the amount of heat which can be extracted from the rock and used for vaporization is a function of the extent of cooling which occurs at the vaporization front and the amount of heat which is conducted towards the point of injection. The heat required to overcome the latent heat of vaporization is supplied by the rock grains within the vapor-saturated thermal boundary layer immediately ahead of the liquid-vapor interface. However, in the case of a fractured system, the heat is supplied by conduction from the fracture walls perpendicular to the flow. In order that boiling may occur, the heat required to overcome the latent heat of vaporization must be supplied over a finite area. As a result, boiling has to occur over a broad two-phase zone rather than a sharp interface. This is in contrast to the case of injection into a porous medium at low degrees of superheat, where the liquid-vapor transition zone can be a narrow interface.

In order to develop a quantitative model of this scenario we have used the TOUGH2 general purpose numerical code (Pruess, 1991) for solving the coupled equations of heat and mass conservation in a fractured-porous type geothermal reservoir. In addition we have conducted a series of experiments in which liquid ether was injected at rates of 10-20 ml/min into a horizontal rough-walled fracture in order to determine whether a two-phase zone does indeed develop as predicted. Ether was chosen as the working fluid since it boils at 34.5^{o}C at atmospheric pressure thereby enabling us to study the boiling process using fracture temperatures of 50-90^{o}C. In Figure 2.3 we show a series of photographs taken at various times during the course of one experiment as ether was injected at constant rate. As the ether migrated radially out into the fracture, a liquid zone developed close to the injection port. Ahead of this zone a two-phase region developed. The leading (front) edge of the two-phase zone is shown in Figure 2.3 by the region of concentrated dye. The orange dye used was only soluble in the liquid phase of ether and therefore accumulated at the edge of the boiling zone as shown. The front was observed to remain roughly circular. The present experimental results provide a reliable data set to test the numerical prediction of TOUGH2. The numerical problem considered for comparison with the experimental observations was a two-dimensional radial system with semi-infinite fracture walls.

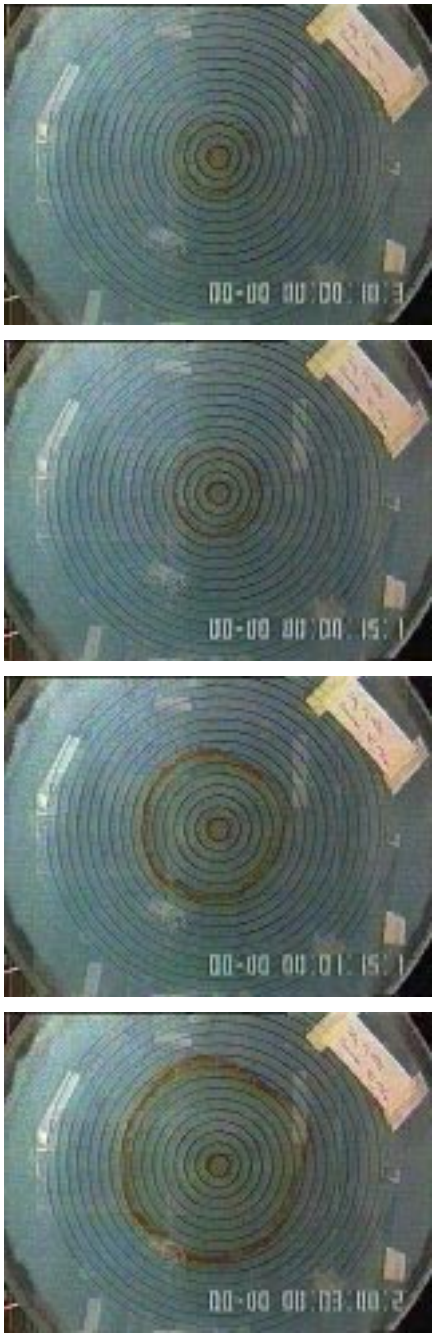

Figure 2.3 The spreading of dyed ether as it is injected at 20ml/min. The times shown correspond to times 10, 15, 75 and 180s after the onset of injection. The region of concentrated dye indicates the leading (front) edge of the two-phase boiling zone.

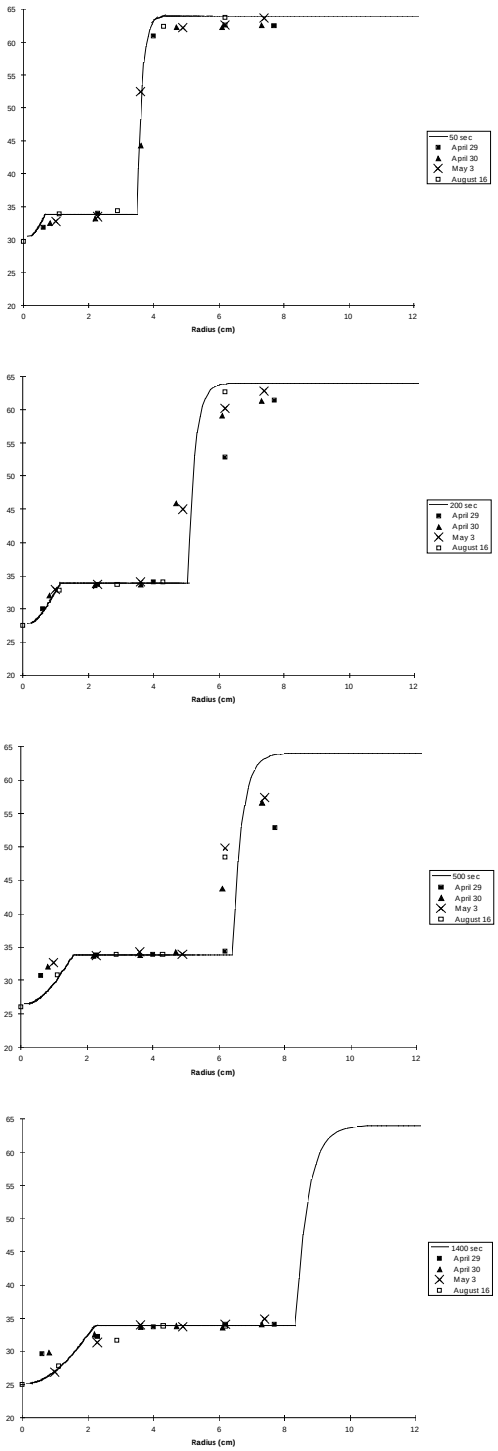

Figure 2.4 Temperature profiles at times 50, 200, 500 and 1400s after the onset of injection of 21°C liquid ether at 10 ml/min into a fracture originally at 64°C. The symbols represent data obtained from different experiments and the solid line indicates the profile obtained from the modified numerical code TOUGH2.

In order to compare the numerical prediction of the code with the experimental results, the code was modified to incorporate the physical properties of ether rather than water for the

reservoir/apparatus fluid. For example, properties of ether at atmospheric conditions include: vapor density 3.331kg/m^3, liquid density 713.8kg/m^3, latent heat of vaporization 377.7kJ/kg, vapor viscosity 8.4e-6 kg/sm and liquid viscosity 1.66e-4 kg/sm (Weast, 1972).

We found that heat was transferred from the brass injection port to the liquid ether. In order to account for this additional heat transfer we placed a thermocouple within the fracture at the point of entry of the fluid. As the experiment proceeded the inlet temperature of the liquid ether to the fracture decreased as expected. Therefore, the inlet temperature of the liquid used in the numerical fracture model was reduced at various times in accord with the experimental observations.

Experiments were conducted at flow rates of 10 and 20 ml/min. Typical temperature profiles at various times for 10 ml/min are shown in Figure 2.4. It is seen that the agreement between the experimental observations and the numerical predictions is good. Close to the injection port a liquid-filled region develops as predicted. Within this liquid-filled zone the experimental data is in very close agreement with the numerical prediction. The radial temperature and temperature gradient increase away from the injection site until boiling conditions are attained. Ahead of the liquid zone lies a two-phase zone. The scatter of the experimental data becomes greater towards the leading edge of the two-phase zone. During the course of the experiments it was found that the leading edge of the boiling zone tended to pulse rather than migrate steadily. As a result, the temperature may have fluctuated whereas the numerical prediction did not indicate this phenomenon. These experimental results suggest that the predictions for the evolution of the temperature, pressure and saturation distributions which one may obtain from TOUGH2 are likely to be very accurate for uniform horizontal fractures bounded by impermeable rock.

2.5 CONCLUSIONS

We have conducted a series of laboratory experiments in order to test the theoretical models of liquid injection into a liquid-filled or superheated porous medium type reservoir (Woods and Fitzgerald, 1993, 1996). In the case of liquid injection into a liquid-filled porous medium we found that at low flow rates, the temperature increases immediately from the injection port in accord with the theory. However, at higher flow rates, an isothermal zone develops close to the inlet site. The liquid is heated to the far-field temperature by cooling the rock close to the source.

We have also performed an experiment in which liquid was injected into a porous rock initially filled with superheated vapor. In this case a sharp interface between the liquid- and vapor-filled regions develops. The amount of heat available for vaporization depends upon the difference in the amount of heat conducted from the vapor-filled zone towards the interface and that conducted away from the interface into the liquid-filled zone. The

experimental results indicate that the theoretical treatment of injection proposed by Woods and Fitzgerald (1996, 1997) is accurate.

We then investigated the case in which liquid is injected into a fracture bounded by impermeable rock in order to ascertain the primary differences between heat transfer and boiling within porous media and fractured systems. It was found that a broad two-phase zone formed within the fracture in order that boiling could occur. This is in contrast to the case of boiling in a porous medium where a sharp interface formed between the liquid- and vapor-filled zones.

We are in the process of developing this work further and will examine experimentally how an injection plume migrates under gravity and how the rate of propagation of the cold water changes when the rock bounding the fracture is permeable.

3 MEASUREMENTS OF STEAM-WATER RELATIVE PERMEABILITY

This project is being conducted by Research Assistant Raul Tovar, Dr. Cengiz Satik and Professor Roland Horne. The aim of this project is to measure experimentally relative permeability relations for steam and water flowing simultaneously in a porous medium.

3.1 SUMMARY

During the quarter, a set of relative permeability relations for simultaneous flow of steam and water in porous media measurements were attempted in steady state experiments conducted under conditions that eliminate most errors associated with saturation and pressure measurements. However, while attempting to measure them the two cores samples used started leaking at the core-epoxy inlet interface. In this report we show the results obtained before the onset of core failure.

3.2 EXPERIMENTAL APPARATUS

The experimental apparatus consisted of an injection unit and a core holder made of epoxy. The injection unit consisted of two furnaces to generate steam and hot water. Two power controllers were used to control the energy supplied by each of the two furnaces. Heat losses along the core body were measured by using eight heat flux sensors. Temperatures were measured by seventeen thermocouples, nine of which were J-type thermocouples, placed along the steam injection, water injection and sink lines. The remaining eight T-type thermocouples and the eight heat flux sensors were placed at equal intervals along the core body. Pressures were measured by using seventeen pressure

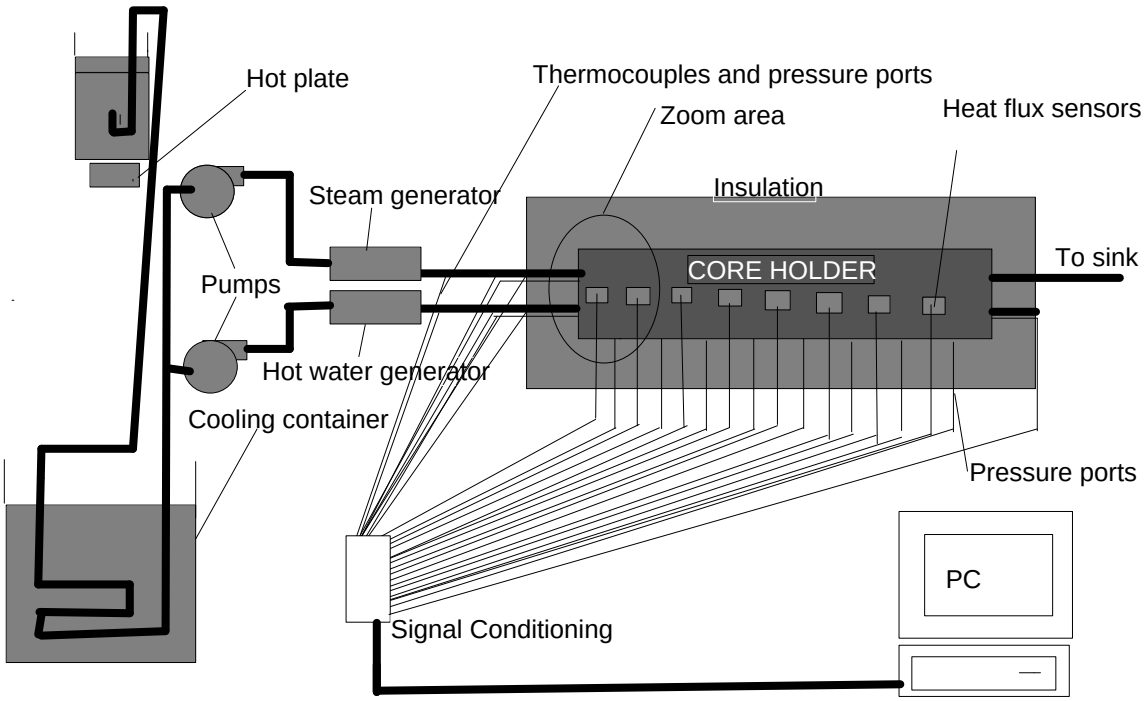

Figure 3.1 Experimental apparatus.

and thermocouples

taps placed next to the thermocouples.

The proportional voltage signals from the heat flux sensors, thermocouples and pressure transducers were first conditioned and then they were collected by a data acquisition system. The data was then analyzed in a personal computer using "LABVIEW", a graphical programming software.

The core (Berea sandstone) samples used for these experiments were 43.18 cm in length and 5.08 cm in diameter. During the preparation of a core holder, core samples were first heated to 450°C for twelve hours to deactivate clays and to get rid of residual water. Eight ports to measure temperatures and pressures were next fitted at fixed intervals along the edge of the core before the rest of the core was covered completely by a high temperature epoxy. The core was tested for leaks before being covered with an insulation material made of ceramic blanket. Experiments were conducted inside a high-resolution X-ray CT scanner so that in-situ saturations could be measured while the experiment was in progress.

Air initially dissolved in the water would give erroneous saturation readings, so air was removed by boiling and cooling the water before injecting into the core, as shown in Figure 3.1. Also, the core was evacuated using a vacuum pump to get rid of the air trapped inside the pore space.

3.3 CALCULATIONS

Mass flowing fractions can be calculated by applying the following mass and energy conservation equations:

$$m_t = m_v + m_l \tag{3.1}$$

$$m_v h_v + m_l h_l = m_t h_t + Q \tag{3.2}$$

where m and h denote mass flow rate and enthalpy, respectively, and the subscript t refers to total, v to vapor phase and l to the liquid phase. Q is the total heat lost upstream of the point being considered.

To apply these equations to the control volume shown in Figure 3.2, at point 1 superheated steam is injected at a know rate m_1, pressure p_1 and temperature T_1. At the same time sub-cooled water is injected at point 2 at a know rate m_2, pressure p_2 and temperature T_2. From T_1 and p_1 using the steam table for superheated conditions we can interpolate to obtain h_{1v}. From T_2 and using the steam table saturated for saturated conditions we can approximate h_2 by using h_{2l}, the enthalpy at the saturated liquid phase. At point 3, when saturation is reached, either from p_3 or T_3 using saturated steam tables we can obtain h_{3l} and h_{3lv}., the liquid phase enthalpy and the latent heat of vaporization respectively. Q is obtained by using Q", *the* heat flux sensor value:

$$Q = Q'' A \tag{3.3}$$

where A is the surface area of the core from point 1 (or point 2) to point 3.

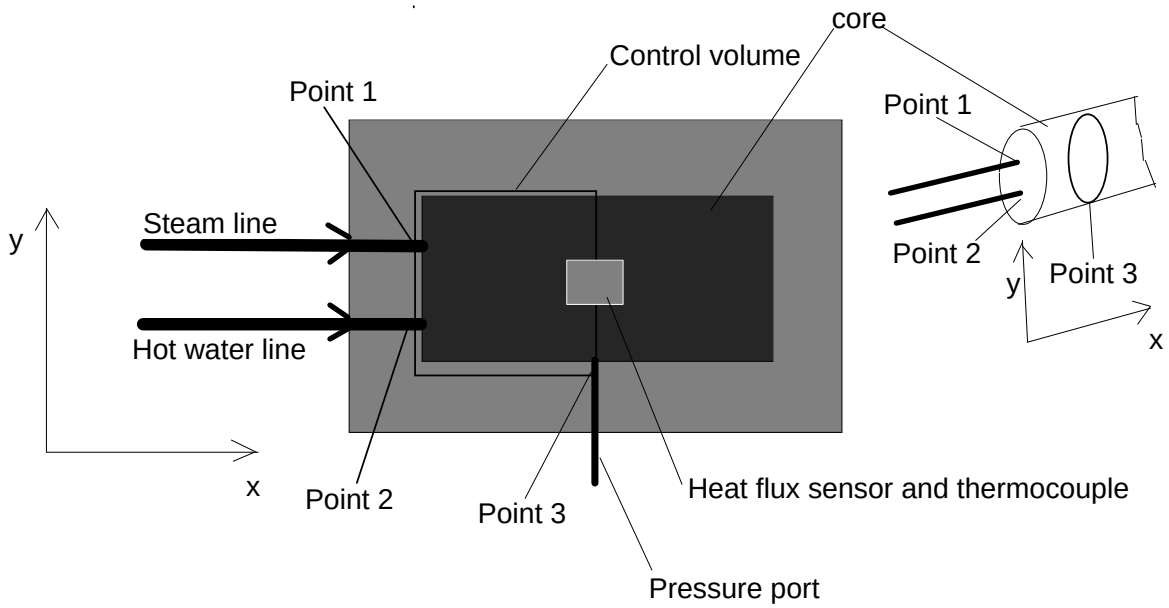

Figure 3.2 Control volume from Figure 3.1 zoom area.

Thus Equation (3.1) becomes:

$$m_3 = m_1 + m_2 \tag{3.4}$$

and (3.2) becomes:

$$m_1 h_{1v} + m_2 h_{2l} = m_3 h_3 + Q'' A \tag{3.5}$$

where:

$$h_3 = h_{3l} + x h_{3lv} \tag{3.6}$$

Thus the steam fraction x in the flow at any time can be calculated by

$$x = \frac{m_1 h_{1v} + m_2 h_{2l} - Q'' A}{m_3 h_{3lv}} - \frac{h_{3l}}{h_{3lv}} \tag{3.7}$$

Then the relative permeabilities to steam and water can be calculated by the corresponding Darcy equations for each phase in terms of the mass flow rates

$$k_{rl} = -\frac{(1-x) m_t \mu_l \nu_l}{kA \frac{\Delta p}{\Delta x}} \tag{3.8}$$

and

$$k_{rs} = -\frac{x m_t \mu_s \nu_s}{kA \frac{\Delta p}{\Delta x}} \tag{3.9}$$

3.3 PRELIMINARY RESULTS

Two core samples were used to generate the following results. Core sample 1 failed before any meaningful X ray CT scan could be taken.

Figure 3.3 shows absolute permeability measured over a time interval of 250 minutes for core sample 1. Each curve represents measurements taken at different temperatures with a constant flow rate. The curves seem to indicate that there is no major variation in permeability as a function of temperature. The variation shown is most probably caused by the precision of the pressure transducers used to measure pressure in the experiment.

Figure 3.4 shows absolute permeability measured over a time interval at different temperatures and flow rates for core sample 2. This figure once again does not show an appreciable variation or permeability with respect to flow nor temperature with the exception of a hike at the third point (about 20 minutes) for the curve with an average permeability of 684 md. The curve with an average permeability of 661 md was obtained as the core was heated from 39 ^{o}C to 88 ^{o}C in a period of 250 minutes.

The pressure drop between the first and the last pressure ports (see Figure 3.1), separated by a distance of 35 cm, was used to calculate the permeabilities shown in Figures 3.3 and 3.4. In both cases the flowing fluid was liquid water. Note that the time intervals for each curve in both figures are independent of each other.

Figure 3.5 shows steady-state measurements along the core sample 2 for a total mass flow rate of 1.03×10^{-4} kg/s. Porosity and steam saturation were obtained using the X-ray CT scanner. Temperature, pressure and heat flux were measured as outlined in section 3.2. The porosity profile given in Figure 3.5a shows no appreciable variation indicating that the core sample is fairly homogeneous.

Table 3.1 shows the estimated steam-water relative permeabilities for the core sample 2. The values for point 1 and 2 were obtained using data from the steam and water injection lines respectively. The values for point 3 were obtained using the data from Figure 3.5 at 4 cm downstream of the core inlet. The calculations were made using Equations 3.3 through 3.9 as outlined in Section 3.3.

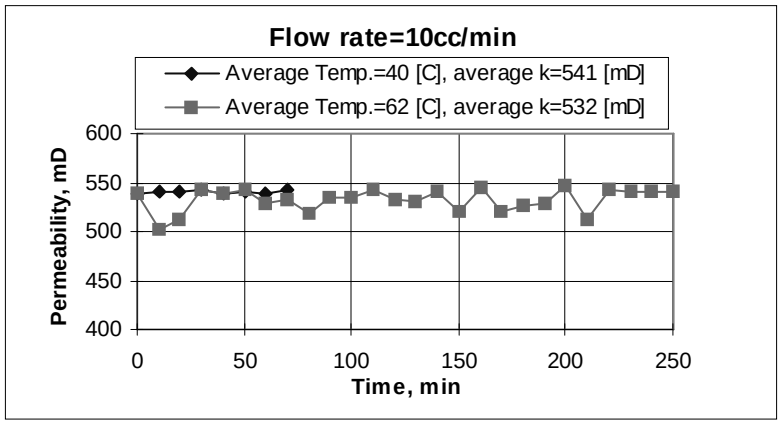

Figure 3.3 Permeability at different temperatures for core sample 1.

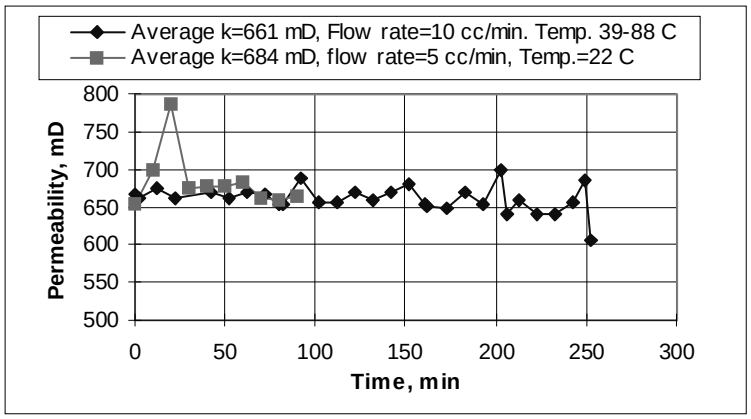

Figure 3.4 Permeability for core sample 2.

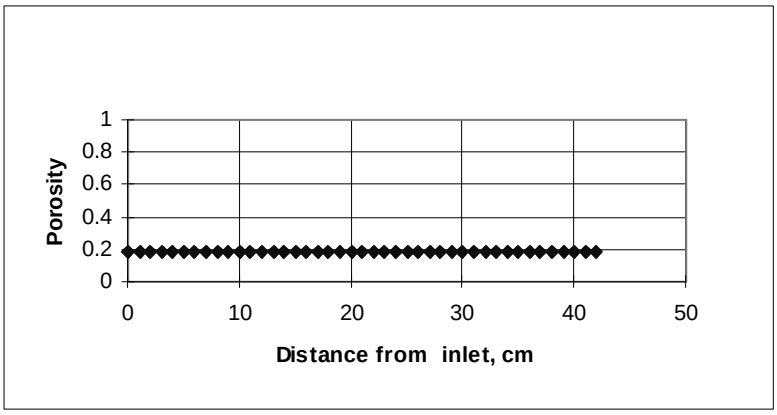

Figure 3.5a Porosity profile for core sample 2.

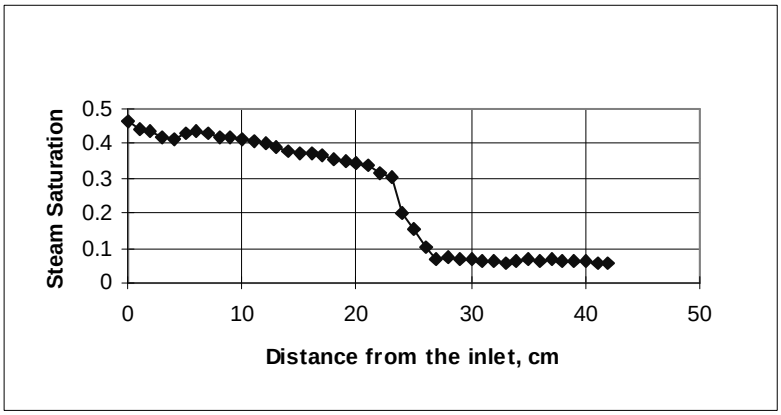

Figure 3.5b Steam saturation profile for core sample 2.

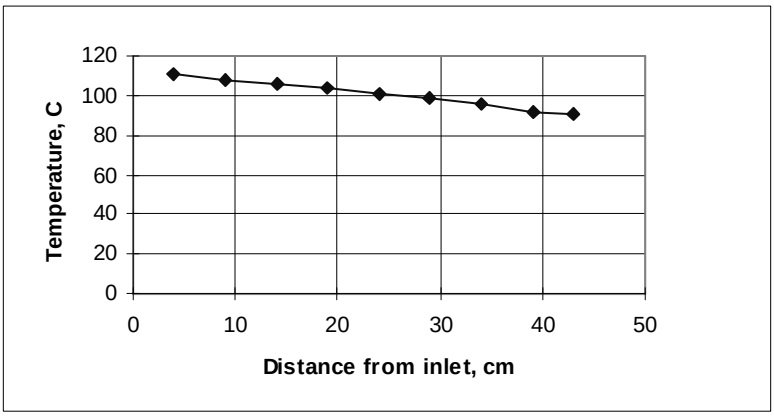

Figure 3.5c Temperature profile for core sample 2.

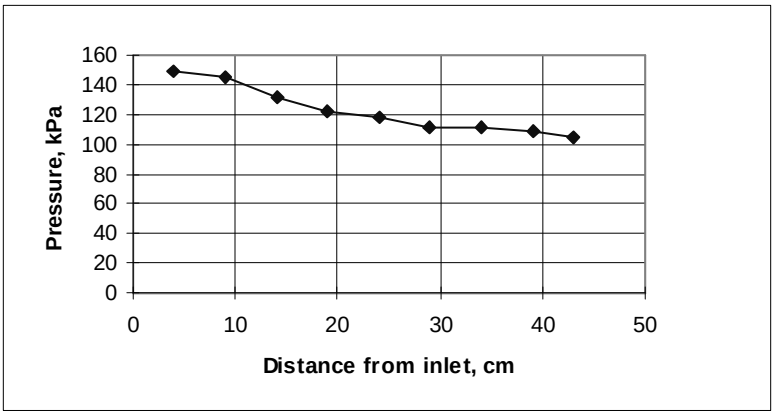

Figure 3.5d Pressure profile for core sample 2.

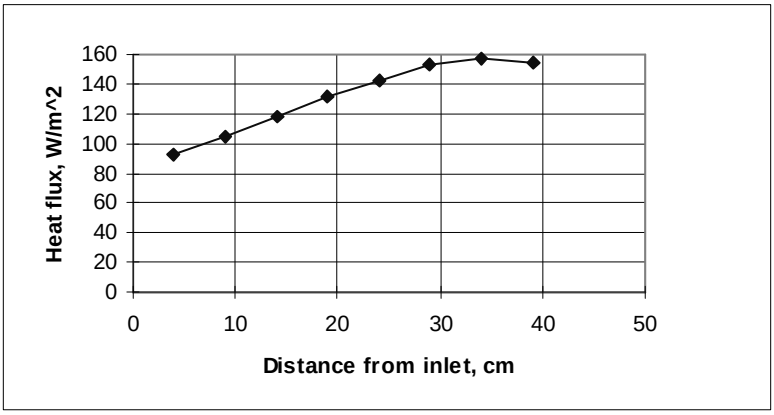

Figure 3.5e Heat flux profile for core sample 2.

Vapor			**Liquid**			**Saturated**			
T_1, C	h_1, Kg/KJ	m_1, Kg/s	T_2, C	h_2, Kg/KJ	m_2, Kg/s	T_3, C	m_3, Kg/s	Q, kW	**h_3, Kg/KJ**
111.8	2664	1.33E-05	111.8	439	9.00E-05	110.6	1.03E-04	7.46E-04	718.24976

Steam quality			**Permeability**
h_l, Kg/KJ	h_{lv}, Kg/KJ	**x**	**k, mD**
439	2225	0.125506	661

Relative permeability							**Water**	**Steam**	**Saturation**
u_l, Kg/ms	v_l, m^3/Kg	u_v, Kg/ms	v_v, m^3/Kg	A, m^2	delp, Pa	L, m	**k_{rl}**	**k_{rv}**	**S, steam**
2.52E-04	0.001052	1.24E-05	1.21	2.07E-03	1.09E+05	0.04	0.00643	0.05222	41%

Table 3.1 Relative permeability calculations and the corresponding steam saturation.

3.4 CONCLUSION

Absolute permeability measurements did not indicate a large variation at different temperatures and flow rates for the two core samples used in the experiments. The small variation observed could be attributed to the precision of the pressure transducers.

Figure 3.5c and 3.5e show that insulation could be improved downstream of the first pressure port. Regardless, Figure 3.5e and Table 3.1 show that heat losses are small compared to the flowing fractions heat capacities, implying a virtually adiabatic core.

The relative permeability measurements shown here are only preliminary since superheated conditions for the steam line could not be checked. Also failure of the core during the experiment did not allow for further measurements to obtain relative permeabilities for a full saturation range. Thus new experiments are needed to obtain a full set of steam/water relative permeability curves. These experiments will be conducted in the coming quarter.

4 NUMERICAL AND EXPERIMENTAL INVESTIGATIONS OF HEAT PIPES IN FRACTURED RESERVOIRS

This study is being conducted by Research Assistant Nemesto Noel A. Urmeneta and Program Manager Prof. Shaun D. Fitzgerald. Geothermal reservoirs are typically highly fractured and the flow of geothermal fluids through these conduits is extremely important in the context of injection and thermal breakthrough. The study is aimed at investigating the effects of capillarity on fluid flow within geothermal reservoirs. This is particularly important in the case of vapor dominated reservoirs since the fractures are usually of high vapor saturation and the transfer of fluid between the adjacent porous matrix and the fracture is an important parameter to consider when designing injection strategies in geothermal reservoirs.

4.1 CURRENT STATUS

The two-dimensional, irregular grid model that was constructed a quarter ago was modified. The current model has dimensions of 7 m x 501 m x 50 m and consists of 220 blocks (Fig. 4.1). The aquifer and the heat sink layers in the previous model were combined into a single layer in the current model. In order to have a constant pressure and

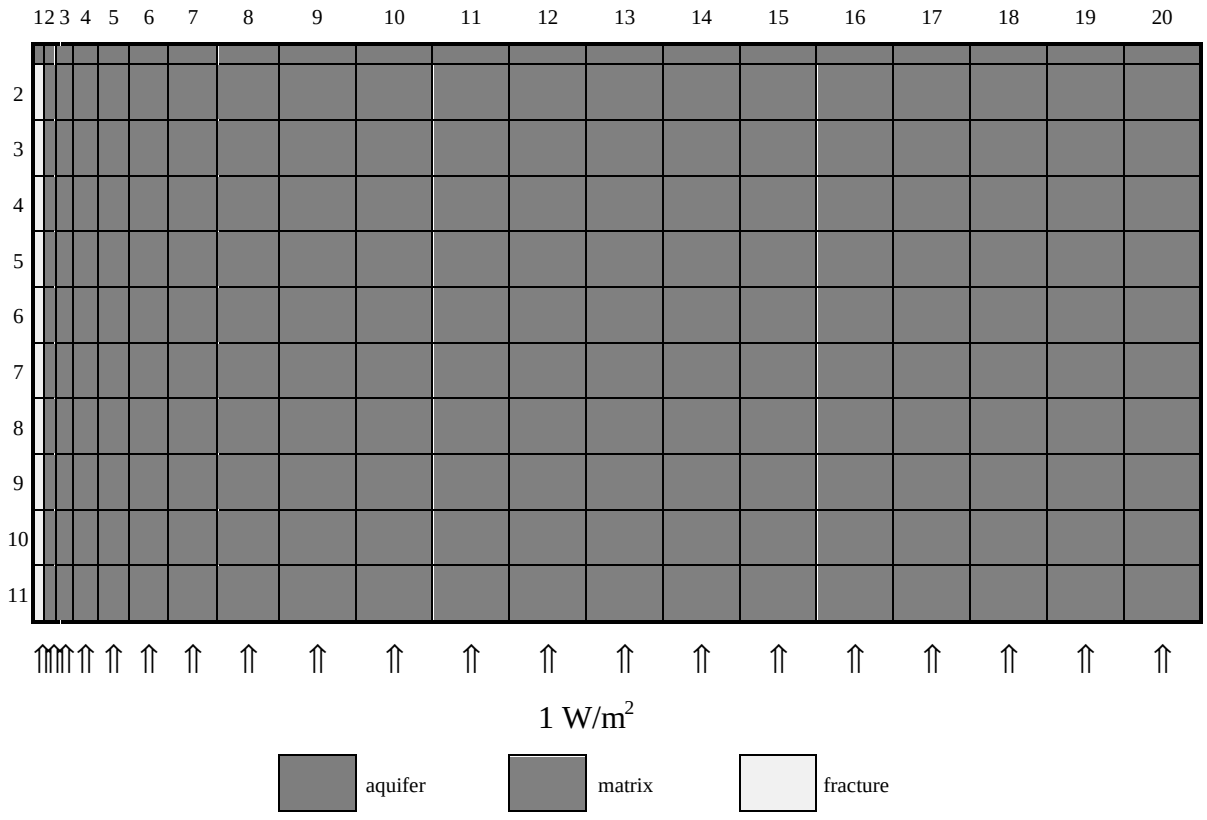

Figure 4.1 The 20 x 11 x 1 block model.

temperature boundary, the blocks in the topmost layer were assigned a very large volume. These blocks have a permeability of 2000 md, a porosity of 0.8, a pressure of 800 kPa and a temperature of 160°C. The matrix blocks were assigned a permeability of 0.5 md and a porosity of 0.1. The fracture blocks were given a permeability of 50 md and a porosity of 0.5.

Hornbrook and Faulder (1993) modeled a fracture by having large blocks (10 m wide) which were assigned a porosity of 0.0001 in order to simulate a 1 mm fracture. They made use of a nine-point differencing scheme. The fracture in this case was modeled by having blocks which are thin (0.01 m wide) and were given a porosity of 0.5 in order to simulate a 0.005 m fracture. A nine-point differencing scheme, as opposed to the regular five-point differencing scheme, was used since Pruess (1991) has shown that a higher-order differencing scheme substantially diminishes the grid orientation effects.

A cubic relative permeability curve was used for all blocks in the model. To investigate the effect of capillary pressures on fluid flow through the fracture and matrix blocks, several capillary pressure curves were utilized. The capillary pressure curves used for the different simulation runs are shown in Figs. 4.2 - 4.5. The matrix capillary pressure is described by the equation

$$P_{cm} = 100\left(S_w^{-1/0.6} - 1\right)^{0.4} \tag{4.1}$$

while the fracture capillary pressure is described by the equation

$$P_{cf} = -A\left(S_w\right) + A \tag{4.2}$$

where S_w is the water saturation and A is the maximum fracture capillary pressure in kPa. The maximum fracture capillary pressures were 200 kPa, 100 kPa, 50 kPa and 0 kPa for Cases 1, 2, 3 and 4, respectively.

Using the numerical simulator TETRAD, the four different cases were ran to steady state. A base case, Case 5, was likewise run to steady state and in this case, no capillary pressure was specified for either the matrix or the fracture blocks.

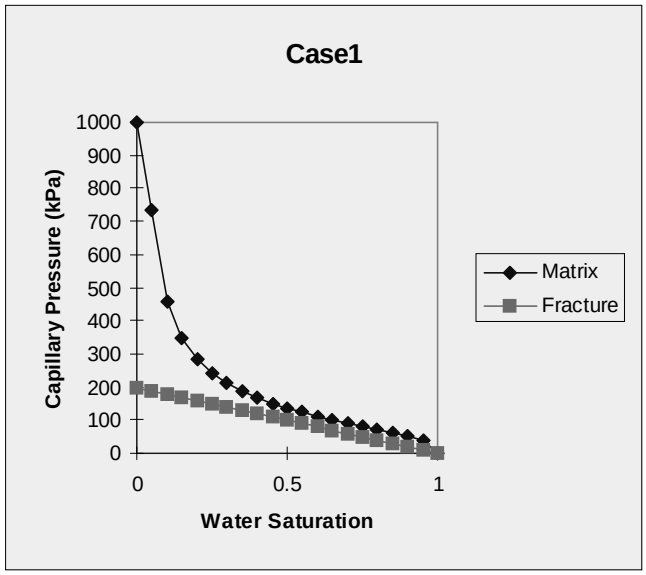

Figure 4.2 Capillary pressure curves for Case 1.

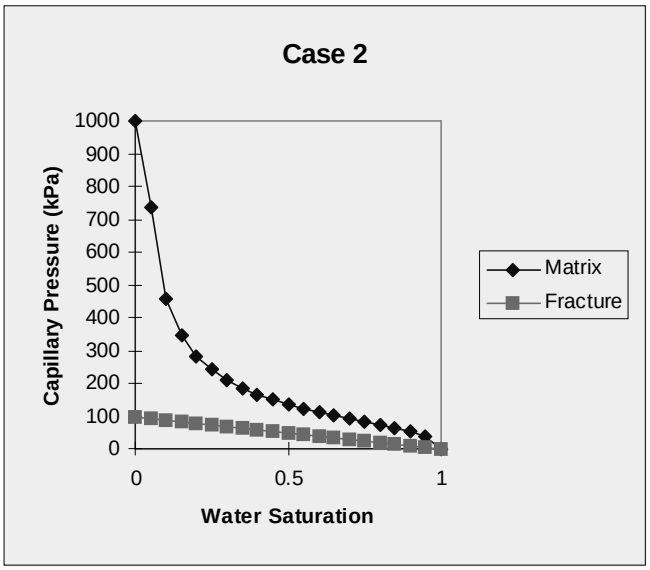

Figure 4.3 Capillary pressure curves for Case 2.

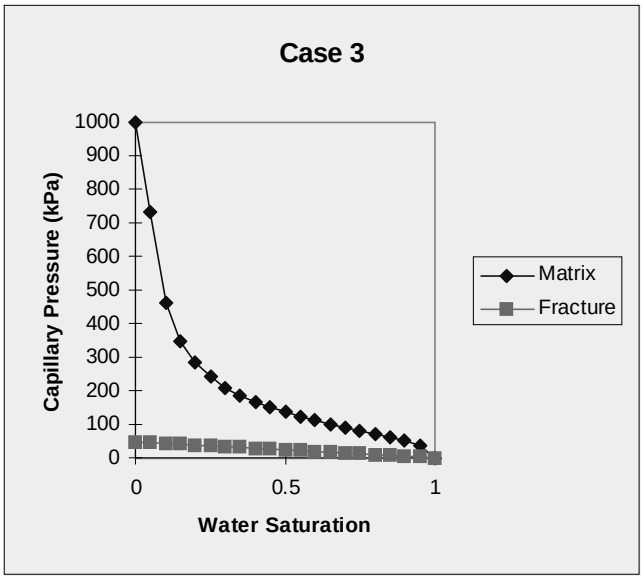

Figure 4.4 Capillary pressure curves for Case 3.

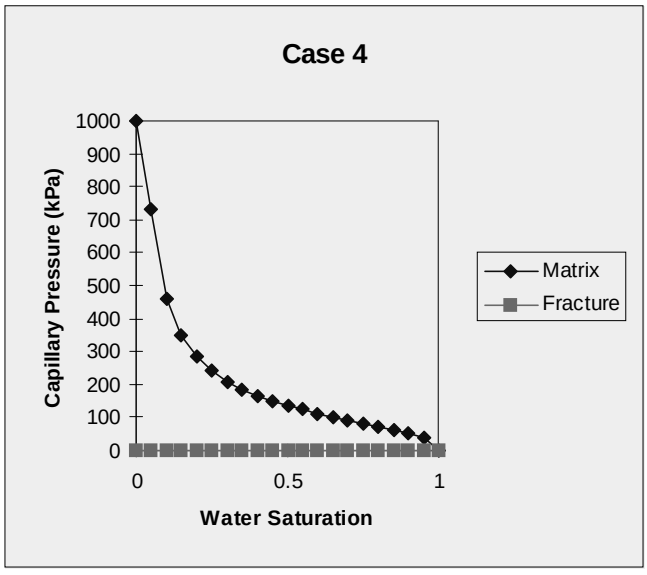

Figure 4.5 Capillary pressure curves for Case 4.

4.2 RESULTS AND DISCUSSION

For all the cases, layers 1 to 7 were liquid-filled. For Case 1, it was observed that layers 8 to 11 were filled up with a two-phase fluid (Fig. 4.6). Decreasing the maximum capillary pressure in the fracture blocks from 200 kPa to 100 kPa resulted in the lowermost block in fracture being completely filled with steam (Fig. 4.7). Lowering the maximum capillary pressure in the fracture blocks resulted in having the two blocks which are steam-filled (Fig. 4.8).

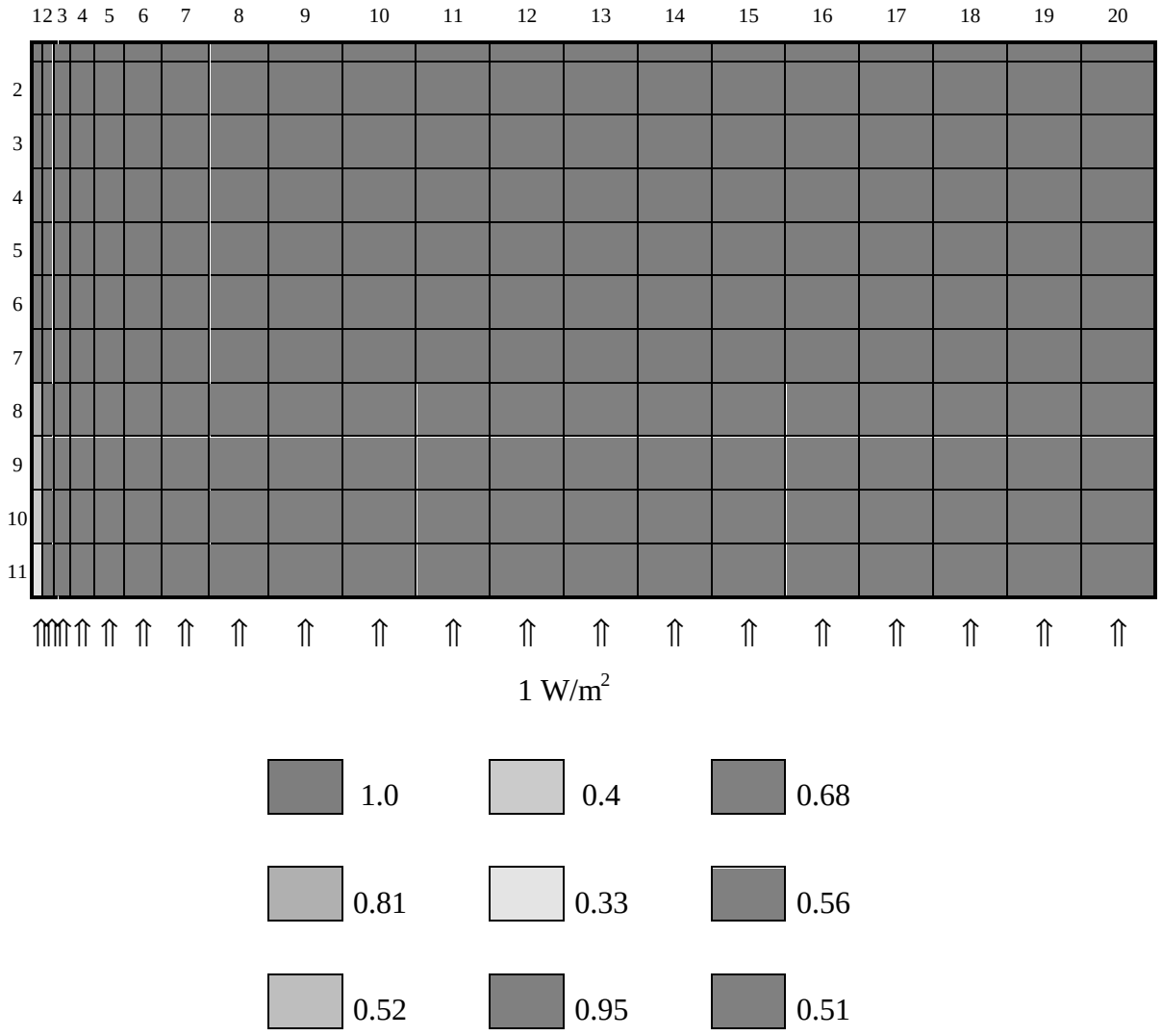

Figure 4.6 Water Saturation: Case 1.

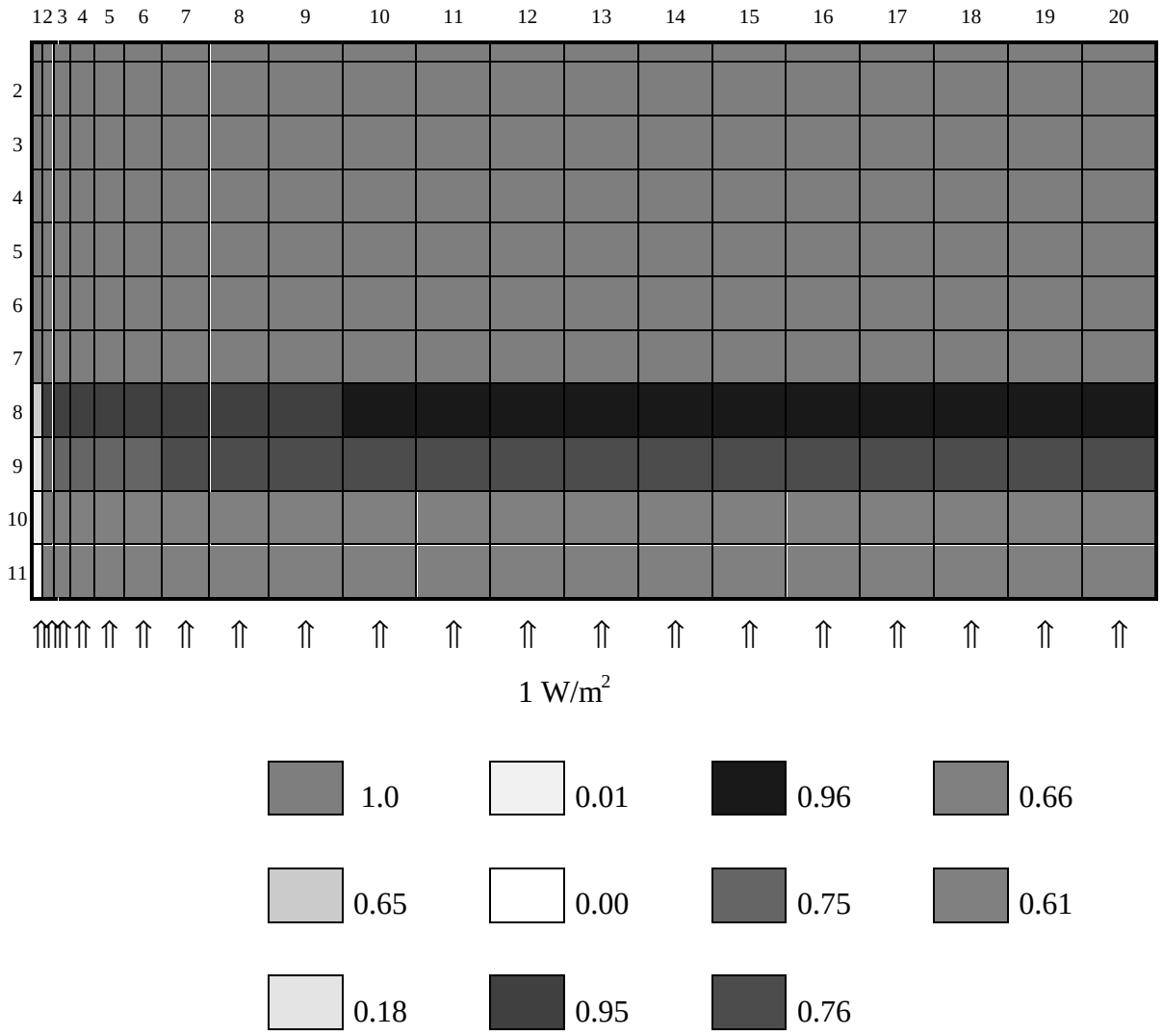

Figure 4.7 Water Saturation: Case 2.

For the case where the capillary pressure in the fracture is zero, it was observed that three of the blocks in the fracture became fully filled with steam (Fig. 4.9). For the base case where no capillary pressures were assigned to both the matrix and fracture blocks, the fracture was observed to be liquid-filled.

Capillary forces do influence the fluid flow between the fracture and the adjacent matrix. In Case 1, the capillary pressure in the fracture was high. Therefore, more fluid is sucked into the crevices, which explains the existence of the two-phase liquid in the fracture. As we lower the maximum capillary pressure, less of the liquid is retained. This accounts for the decrease in water saturation and the development of steam-filled fracture blocks.

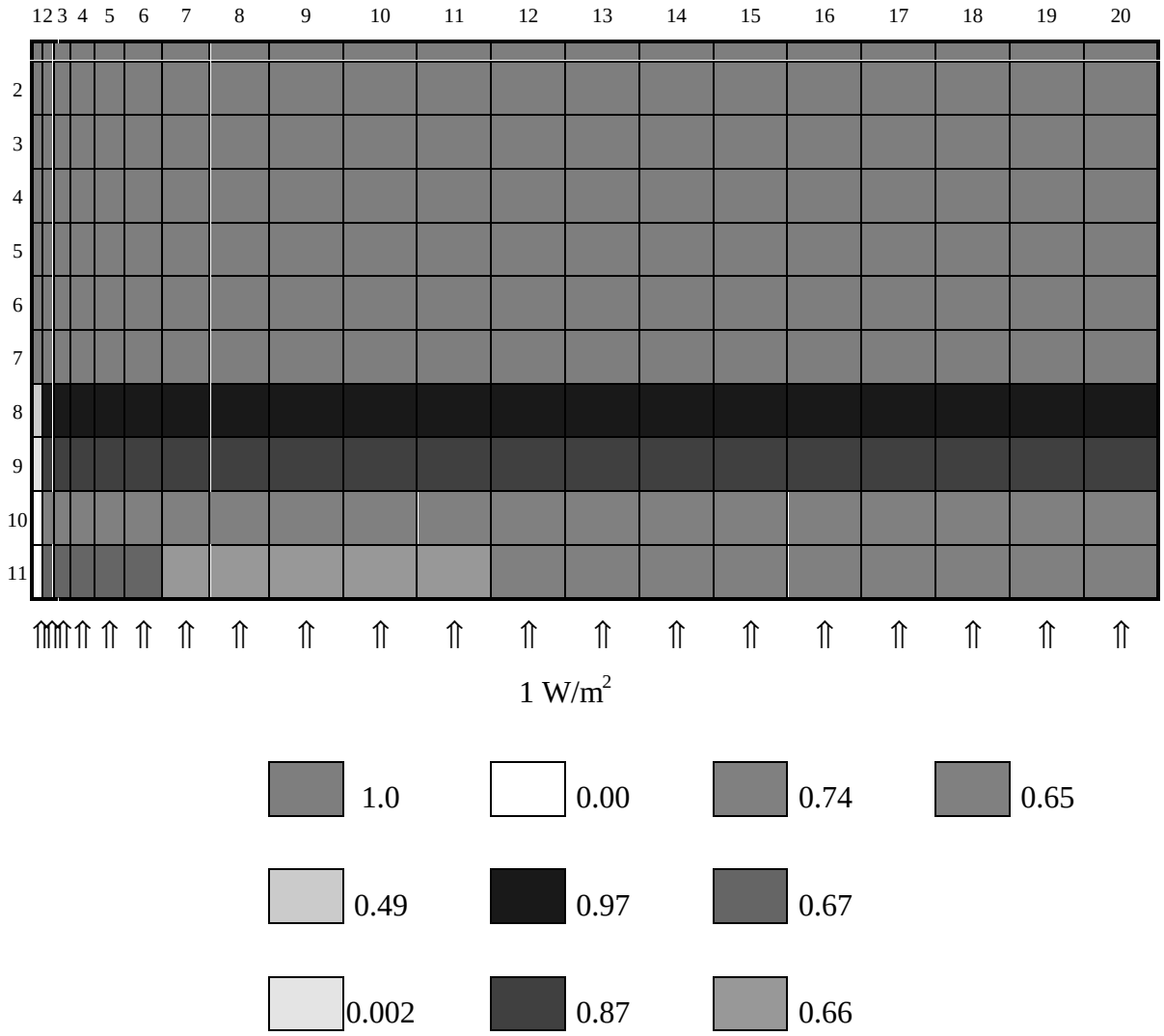

Figure 4.8 Water Saturation: Case 3.

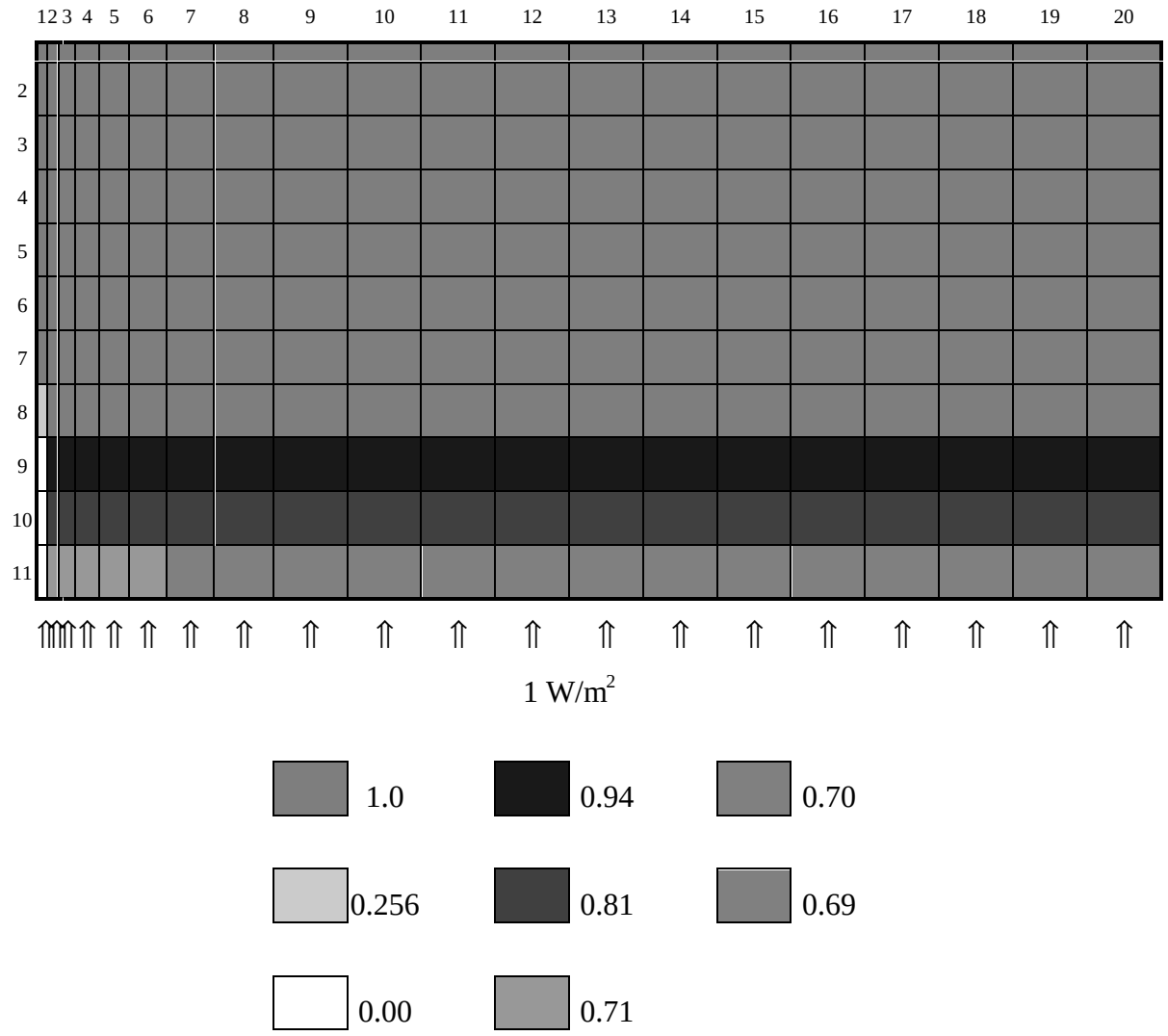

Figure 4.9 Water Saturation: Case 4.

4.3 SUMMARY

The fracture was modeled by thin blocks which were given a high porosity value and a relatively high permeability. A nine-point differencing scheme was used when numerical simulations were carried out with TETRAD in order to minimize the grid orientation effects. To investigate the effect of capillary forces, several capillary pressure curves were assigned to the matrix and fracture blocks. With the two-dimensional model, we were able to observe the effects of capillary forces on the state of the system. These results are preliminary. A more detailed observation on the effects of capillary pressures on fluid flow will be conducted in the next quarter.

5 MODELING OF GEOTHERMAL RESERVOIRS CONSTRAINED TO INJECTION RETURN DATA

This project is being conducted by Research Assistant Ma. Michelle Sullera and Prof. Roland Horne . It aims to deduce the injection return mechanisms and flow paths from correlations between chloride concentration at producing wells and operating parameters (flow rate and injection chloride) at injection wells.

5.1 BACKGROUND

Traditionally, tracer tests are used to establish the degree of connectivity between wells. However, for wells which are only weakly connected these tests may need to be conducted over long periods of time using huge amounts of tracer of sufficient stability to obtain meaningful data. In such cases tracer tests would be too costly and impractical.

On the other hand, there are substances naturally occurring in the reservoir which behave like tracers. One such substance is chloride. In Palinpinon, a geothermal field in the Philippines, some injectors and producers are sufficiently strongly connected that changes in injection rates result in corresponding increases or decreases in produced chloride concentrations. The magnitude of the changes in chloride concentration reflect the degree of communication between the wells. Moreover, chloride is stable, conservative; and free. We can therefore extract the same, if not more, information from chloride data as we could from traditional tracer tests, at lower cost. This is just what this project proposes to do.

Specifically, this project aims to identify possible flow paths and injection return mechanisms from analysis of chloride production data and injection data in producing geothermal fields.

5.2 MODELING APPROACH

Following is a very general approach to the problem: First, seek a correlation between chloride concentrations in production wells and injection rates. Second, deduce mechanisms, consistent with the previously obtained correlation, by which injectate returns to the reservoir and is reproduced. Then, verify the accuracy of these mechanisms by incorporating them into a simulation model of the reservoir and generating history matches.

As the first step of this work, during the current quarter, production and injection data from Palinpinon-I geothermal field were analyzed. To quantify the degree of connectivity

between producers and injectors in the said field, it was initially postulated that there is a linear relationship between produced chloride concentration and injection rates:

$$\mathbf{Cl_P = a_0 + a_1Q_{I1} + a_2Q_{I2} + a_3Q_{I3} + ... \quad ... + a_nQ_{In}} \qquad \text{CORRELATION 1} \qquad (5.1)$$

where $\mathbf{Cl_P}$ = chloride concentration in production well, P

$\mathbf{Q_{In}}$ = mass flow rate to injection well, In

$\mathbf{a_n}$ = linear coefficient of well In

$\mathbf{a_0}$ = a constant associated with local chloride concentration

A high value of $\mathbf{a_n}$ indicates a strong connection between producer P and injector I_n.

Recognizing that apart from its dependence on injection rates chloride concentration also has a natural tendency to increase with time as the reservoir is produced, a second correlation with an additional linear term in time was proposed:

$$\mathbf{Cl_P = a_0 + a_1Q_{I1} + a_2Q_{I2} + a_3Q_{I3} + ... \quad ... + a_nQ_{In}} + ct \qquad \text{CORRELATION 2} \qquad (5.2)$$

5.3 RESULTS AND DISCUSSION

Using production data from Palinpinon, values of the linear coefficients in Eqn. (5.1) and (5.2) were calculated and predicted values of chloride plotted against actual data. Results for two typical production wells are shown in Figs. (5.1) and (5.2).

One interesting result is that some of the coefficients had negative calculated values. This implies that the operation of injection wells corresponding to those negative coefficients can actually lessen the percentage of injectate being produced at some locations. One plausible physical explanation is that the injectors with negative coefficients could be diverting the flow from the other injectors away from the production well.

Comparing Figures (5.1) and (5.2), we note that correlation 2 fits the data better than correlation 1. To test how well correlation 2 can predict chloride concentrations, only the portion of the data set spanning 1983 and 1986 was used to calculate the coefficients, then chloride concentrations for the succeeding two years were predicted. Figure 5.3 shows that correlation 2 (Eqn. 5.2) matches the portion of the data used for calculating the coefficients fairly well but overpredicts and underpredicts the chloride concentration for the next two years for wells P1 and P2, respectively.

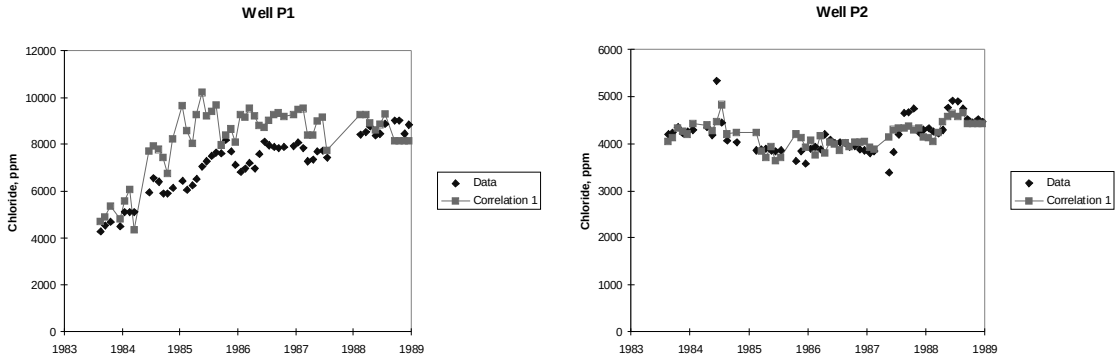

Fig. 5.1 Actual vs. predicted chloride concentration using Eqn. 5.1

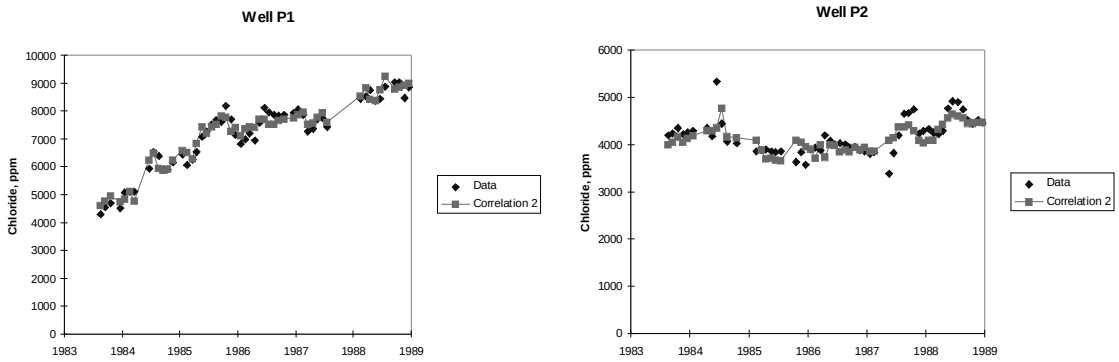

Fig. 5.2 Actual vs. predicted chloride concentration using Eqn. 5.2

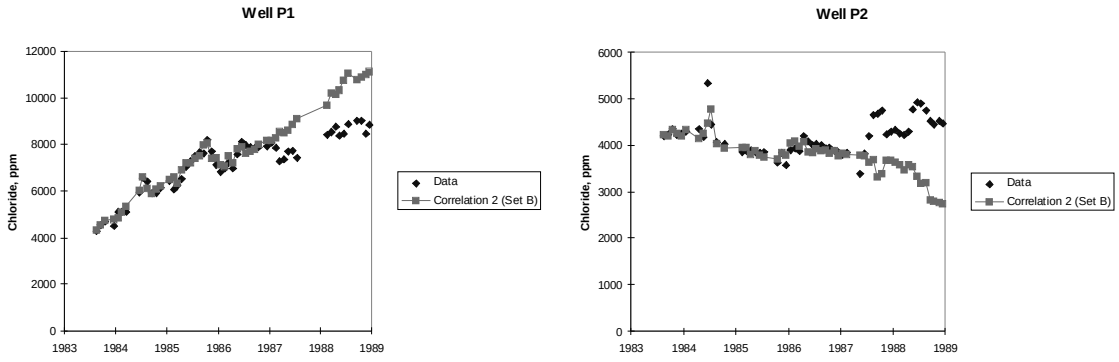

Fig. 5.3 Actual vs. predicted chloride concentration using Eqn. 5.2, 1983-1986 data

5.4 FUTURE PLANS

Correlation 2 gave a good match over the range of data where the coefficients were calculated from but displayed poor predicting capability. The next step will be to see if the incorporation of additional data could improve the predictive capacity. Also, a nonlinear model of chloride concentration with time will be incorporated to account for the fact that chloride does not increase indefinitely with time. After arriving at a satisfactory correlation, we plan to incorporate it with the reservoir model and generate production history matches to test its accuracy.

6 EVALUATION OF SUB-SCALE HETEROGENEITIES IN GEOTHERMAL ROCKS

This project is being conducted by Research Assistant Meiqing He, Dr. Cengiz Satik and Professor Roland Horne. The aim of this project is to identify and characterize fractures existing in geothermal rocks by using X-ray computer tomography (CT) equipment. The description of water or steam's propagation in heterogeneous porous media is currently poorly understood, and in particular the effect of fractures on water or steam distribution, especially under geothermal reservoir condition, is still unknown. There are several concerns related to the necessity of evaluating of heterogeneity of rocks. From previous experiments it has been found that adsorption and the distribution of water or steam in a network consisting of small fractures are not negligible in mass transfer processes, even in fractures with aperture of order 1μm.This research will attempt to elucidate the factors governing liquid and vapor propagation in heterogeneous porous media. Particular emphasis is given to the characterization of rock heterogeneity by using X-ray CT imaging technique in order to obtain a complete understanding of water and steam saturation in heterogeneous and fractured rocks under geothermal reservoir conditions.

The general goal is to advance the understanding of heterogeneity and evaluate its impact on mass transfer. The specific goals are as follows:

- Investigate X-ray CT imaging techniques to improve precision in the measurements of saturation and porosity of fractured and very heterogeneous rocks.
- Characterize the fracture geometry of rock samples from the Geysers geothermal field using the X-ray CT scanner.
- Extract information about pore space from X-ray attenuation coefficients which depend on the density of material and the energy level used during the experiments. In this regard, we will experiment with multiple energy scans for the first time.

6.1 X-RAY CT TECHNIQUE AND APPLICATION

X-ray computerized tomography (CT) is a non-destructive measurement technology that can produce a higher resolution internal image of an object than conventional X-ray methods. It has been commonly applied in the study of rock properties. Unit elements in the generated two-dimensional image matrix generated by the X-ray CT scanner are referred to as CT numbers. Each CT number corresponds to the average attenuation coefficient (μ_{voxel}) within a voxel. The object is divided into cubic voxels which can be thought of as pixels with a thickness. The thickness of a voxel is equal to the slice thickness (X-ray beam thickness) and the square dimension of a voxel is defined by the length of the detectors divided by the dimension of the image matrix which is a result of the sampling rate.

Prior to display of a CT image, it is conventional in the medical field to normalize the X-ray attenuation data to water in the following fashion:

$$CT = \frac{2048(\mu_{voxel} - \mu_{water})}{\mu_{water}} \quad \textbf{(6.1)}$$

where μ is the X-ray attenuation coefficient and CT is the CT number, the unit of which is called a Hounsfield. This equation results in CT numbers of -1024 Hounsfield for air, 0 Hounsfield for water, and 1024 Hounsfield for bone.

The relationship between detected intensity I_d and incident intensity I_0 can be expressed as

$$I_d(x, y) = \int I_0(\varepsilon) \exp\left[-\int \mu(x, y, z, \varepsilon) dz\right] d\varepsilon \quad \textbf{(6.2)}$$

where $I_0(\varepsilon)$ is the incident X-ray beam intensity as a function of the energy per photon ε and μ(x, y, z, ε) is the linear attenuation coefficient at each region of the object. The μ of all materials depends on the photon energy of the beam and the atomic number of the elements in the material (Johns and Cunnigham, 1974). X-ray energy is quantumized into photons. The decrease in the intensity of the X-ray beam after traversing an object is described by the photon absorption or scattering. Attenuation mechanisms are composed of coherent or Rayleigh scatter, photoelectric absorption, and Compton scatter in the diagnostic range, below 200 kev (kilo electron volts).

$$\mu = \mu_R + \mu_P + \mu_C \quad \textbf{(6.3)}$$

Photoelectric absorption dominates in materials with higher atomic-number material. The attenuation coefficient undergoes a sharp increase in the energy region corresponding to the K shell. For high atomic-number material, the K absorption edge occurs within the spectrum of interest. On the other hand, Compton scatter dominates in low atomic-number material, such as water and soft tissue (Macovski, 1983). Regarding the materials of geothermal interest, namely water, steam and rock, only the Compton effect and photoelectric adsorption are expected to be dominant while coherent scatter only happens when the X-ray energy is of the order of a few kev which is not within the energy level range of our experiment. The Compton attenuation contribution μ_C to the total attenuation is dependent on the energy μ, but independent of atomic number. The photoelectric component is dependent on both atomic number and energy level. In order to inspect the appropriateness of the CT numbers generated by our equipment, we wrote code to check the value by tracing the saturation calculation process. Some CT numbers were found to be out of reasonable range under some experimental conditions. We refer to these as

"noise". Instead of simply disregarding those numbers we are trying to uncover the possible mechanisms of any errors in the imaging system and to find an approach to correct for these effects.

6.2 PLAN FOR FUTURE WORK

Since our CT scanner system was originally manufactured for medical uses, there are some data processing algorithms which might not be optimal for our study object (core). We will seek more appropriate algorithms than the one chosen currently to correct beam hardening effect when scanning human bone. Our approach to determine heterogeneities in the cores as well as their saturation distributions by running multilevel energy scans will be established on the relationship between the material's attenuation coefficients and the energy level of the CT scan (Huang, Ringrose and Sorbie, 1996)

7 STUDY OF HEAT TRANSFER AND BOILING IN A FRACTURE

This new research initiative has been conducted by Robert DuTeaux under the guidance of Dr. Shaun Fitzgerald and Dr. Cengiz Satik. The project was developed to improve our understanding of heat transfer and boiling in a discrete fracture by the concomitant development of an experimental apparatus and a numerical model.

7.1 SUMMARY

The initial work on this project has involved the conception and design of an experimental apparatus. A review of literature provided a moderate background of information that will be relevant to the verification of the apparatus with single phase flow and heat transfer, however, only limited experimental or numerical work with liquid injection and boiling in a discrete fracture has been conducted previously. The ultimate objectives of this research will be to analyze the temperature gradients adjacent to a fracture caused by liquid injection and boiling in that fracture, and to understand the movement of the liquid-vapor interface as heat is depleted from the solid medium by conduction to the fracture and convection in the direction of flow with the fluid. An explanation of the apparatus design with a brief projection of the future work follows.

7.2 EXPERIMENTAL APPARATUS DESIGN

The physical properties of the materials used to model fluid flow, heat transfer, and phase change in a discrete fracture have been selected to be similar to the physical properties of rock, and water was selected as working fluid in the design. It was agreed that the cylindrical annulus formed between two large diameter concentric glass tubes best simulated a parallel plate fracture geometry and removed the end-effects of simply using two flat plates. Figure 7.1 illustrates the design that was developed.

The diameter of the core in Figure 7.1 is slightly more than five inches and the height of the assembly is eighteen inches. The core of the apparatus contains thermocouples embedded in sand (or another medium) completely enclosed in glass so that fluid may only flow in the annulus formed by the two concentric glass tubes. The annulus between the glass tubes is approximately two millimeters wide. Outside the larger glass tube is a third concentric acrylic tube with two functions. It allows an insulating vacuum around the apparatus and also serves to contain the glass for safety. At the end of this first quarter of this research the materials needed for the assembly had been acquired and the apparatus was almost ready for construction.

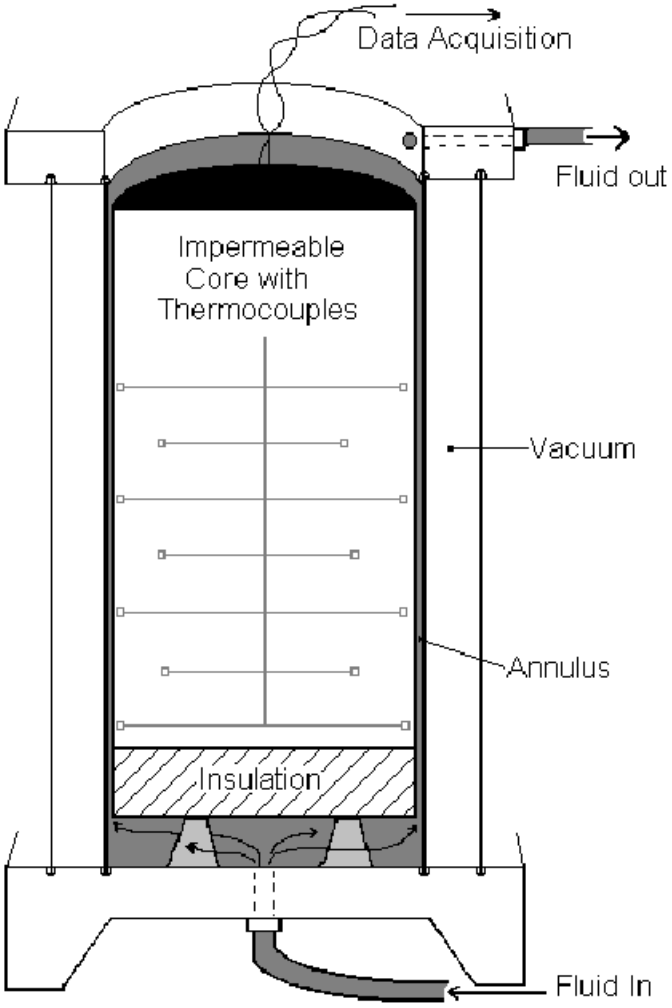

Figure 7.1 The experimental apparatus design.

7.3 NUMERICAL MODELING

This experimental assembly was intended not only for analysis by empirical observation, but also was intended to provide data for comparison to a numerical model yet to be developed. For the case where heat is transferred radially and axially to the surface of a cylinder with a transient surface temperature distribution there is no exact analytic solution. It was decided, therefore, to simulate this phenomenon numerically. Subsequent reports will document further progress towards this goal.

7.4 FUTURE PLAN

In the next quarter, the apparatus will initially be used to obtain data for single phase flow and heat transfer which will be used to evaluate the quality of the experimental design by comparison to numerical simulation. Also, different materials will be used to make the core of the assembly and different thermocouple patterns will be tried. After sufficient trials the apparatus will be used to observe boiling by placing a heated core into the assembly and injecting saturated water into the base and up the annulus. The flow will be controlled at various constant flow rates, and also under constant pressure conditions with an atmospheric outlet pressure. Our future plans also include encoding a two-phase numerical simulation.

8 PRODUCTIVITY VARIATION DUE TO PHASE CHANGE

This research project is being conducted by Research Assistant, Marilou Guerrero, Prof. Shaun Fitzgerald, and Prof. Roland Horne. The purpose of this study is to improve our understanding of productivity index variation due to phase change in geothermal reservoirs by analytical and numerical methods.

8.1 INTRODUCTION

The calculation of productivity index in present reservoir simulators is basically only for single-phase flow. In geothermal systems, however, boiling occurs as pressure drops (i.e. in the case of a water-dominated reservoir). When this happens, the productivity index may no longer be a function of wellbore geometry and permeability. It can vary with time, as geothermal fluids are withdrawn from the reservoir. Thus, it is the objective of this research project to investigate the appropriateness of the commonly used pressure drop equations for two-phase flow into geothermal wells. This will impact economic value of geothermal projects, and therefore is an important aspect of project evaluation.

This report will describe a brief literature review, derivation of governing equations for physical processes in geothermal systems, and discussion of future work.

8.2 REVIEW OF RELATED LITERATURE

In reservoir simulation, pressure at a grid point is taken as the average of the pressure of the block surrounding the grid point. However, for large grid block sizes, a well located in this block cannot use the calculated pressure of the block. One of the techniques developed to solve this problem is by using analytical well models.

Schwabe and Brand (1967) developed their analytical model for single-phase flow from the radial form of Darcy's law. In the absence of skin effect, it is simplified to

$$q = 2\pi kh\,(p_o - p_{wf}) / [\mu\ \ln(\Delta x/r_w)] \qquad (8.1)$$

where k is the permeability, h is the reservoir thickness, p_o is the simulator well block pressure, p_{wf} is the flowing wellbore pressure, μ is the fluid viscosity, Δx is the grid block spacing, and r_w is the wellbore radius. For large grid blocks, van Poolen *et al* (1968) suggested that

$$q = 2\pi kh\,(p_o - p_{wf}) / [\mu\ \ln(\Delta x/(r_w\sqrt{\pi})) - \tfrac{1}{2}] \qquad (8.2)$$

The basic assumption here is that well block pressure is the areal average pressure.

A productivity index, PI, can be defined as

$$q = PI\,(p_o - p_{wf})/\mu \qquad (8.3)$$

Using the expression for q in Equation (8.2),

$$PI = 2\pi kh / [\ln((\sqrt{\Delta x\,\Delta y}/\pi)/r_w) - ½] \quad (8.4)$$

This expression is similar to the productivity index defined by Coats *et al* (1974).

In 1978, Peaceman showed that the well block pressure is equal to the actual flowing pressure at a radius, r_o, for a square grid block. This is expressed as

$$r_o = 0.2\,\Delta x \quad (8.5)$$

Defining r_o as the equivalent wellbore radius, or that radius at which the steady-state flowing pressure of the actual well equals the numerically calculated pressure for the well block,

$$q = 2\pi kh\,(p_o - p_{wf}) / [\mu\ \ln(r_o/r_w)] \quad (8.6)$$

Comparing Equations (8.2) and (8.6) gives

$$r_o = 0.342\,\Delta x \quad (8.7)$$

This result is based on the assumption that the well block pressure is equal to the areal pressure; and it contradicts Peaceman's conclusion that $r_o = 0.2\,\Delta x$.

Furthermore, Peaceman (1982 1983) showed that for a uniform rectangular grid

$$r_o = 0.14\,\sqrt{(\Delta x^2 + \Delta y^2)} \quad (8.8)$$

for single-phase flow.

8.3 GOVERNING EQUATIONS

The general governing equations presented here consist of mass and thermal energy balances for the steam and water phases present in a geothermal system. Assuming steady-state conditions, these balance equations are reduced to two nonlinear partial differential equations:

$$[-M/2\pi dk][1/r\,(\partial p/\partial r)] = \rho_L S^n/\mu_L + \rho_V(1-S)^n/\mu_V \quad (8.9)$$

$$[-M/2\pi dk][1/r\,(\partial p/\partial r)] = 1/C_L T_H\,\{\rho_L S^n C_L/\mu_L\,[T^* + (\partial T/\partial p)_{sat}(p-p^*)] + \rho_V(1-S)^n/\mu_V\} \quad (8.10)$$

where M is the total mass flux, d is the reservoir thickness, k is the formation permeability, r is the distance from a constant pressure boundary to the wellbore, p is the reservoir pressure, C is the specific heat, T_H is the temperature of the single-phase water coming from the boundary, ρ is the fluid density, μ is the fluid viscosity, T* is the reservoir temperature at a reference point, p* is the reservoir pressure at a reference point, and S is the water saturation. Variables with subscript "L" refers to the water phase, while those with subscript "V" refers to the steam phase.

8.4 FUTURE WORK

The ultimate goal of this project is to formulate an equation for productivity index that takes into account boiling or phase change in geothermal reservoirs. To verify this equation, the reservoir simulator TOUGH2 will be used. A section code will be written to adjust the productivity calculation in the simulator.

REFERENCES

1. Fitzgerald, S.D. and Woods, A.W. 1994 The instability of a vaporization front in hot porous rock. *Nature* **367**, 450-453.
2. Hornbrook, J. W. and Faulder, D. D. (1993) Parametric analysis of factors affecting injection and production in geothermal reservoirs. *Proc. Stanford Geoth. Workshop* **18**, 53-60.
3. Huang,Y., Ringrose, P.S. and Sorbie, K.S., "X-ray Imaging of Waterflood Fluid Saturation in Heterogeneous Rock Slabs", SPE 30000, presented at the 1996 SPE Annual Meeting, Denver, CO, pp. 483-495.
4. Johns, J.R., Steude, J.S., Castanier, L.M. and Roberts, P.V., 1993, "Nondestructive Measurements Of Fracture Aperture In Crystalline Rock Core Using X-Ray Computed Tomography", *J. Geophys. Res.*, **98**(B2), 1889-1900
5. Johns, R.A., "Diffusion and Dispersion of Solute in a Variable Aperture Fracture", 1991, PhD dissertation, Stanford University
6. Macovski, A. (1983), "Medical Imaging System", Prentice Hall
7. Pruess, K. (1991) Grid orientation and capillary pressure effects on the simulation of water injection into depleted vapor zones. *Geothermics* **20** (No. 5/6), 257-277.
8. Pruess, K. 1991 *TOUGH User's Guide*. Earth Sci. Div., Report LBL-20700, Lawrence Berkeley Laboratory.
9. Pruess, K., Calore, C., Celati, R. and Wu, Y.S. 1987 An analytical solution for heat transfer at a boiling front moving through a porous medium. *Int. J. Heat Mass Transfer* **30**(12), 2595-2602.
10. Satik, C., 1994, "Studies In Vapor-Liquid Flow In Porous Media", *Ph.D. Thesis*, University of Southern California, Los Angeles, CA
11. Satik, C., Ambusso, W., Castanier, L.M. and Horne, R.N., 1995, "A Preliminary Study of Relative Permeability In Geothermal Rocks",*Trans. GRC*, **19**, 539
12. Satik, C. and Yortsos, Y.C., 1996, "A Pore Network Study Of Bubble Growth In Porous Media Driven By Heat Transfer", *J. Heat Transfer*, **118**

13. Satik, C. and Horne, R.N., 1996, "An Experimental Study of Boiling In Porous Media", *Trans. GRC,***20**, 839

14. Weast, R.C. 1972 *Handbook of Chemistry and Physics*. Chemical Rubber Co.

15. Woods, A.W. and Fitzgerald, S.D. 1993 The vaporization of a liquid front moving through a hot porous rock. *J. Fluid Mech.* **251**, 563-579.

16. Woods, A.W. and Fitzgerald, S.D. 1996 The effects of heat conduction on the vaporization of liquid invading superheated permeable rock. *Proc. Stanford Geothermal Reservoir Engineering Workshop* **21**, 421-425.

17. Woods, A.W. and Fitzgerald, S.D. 1997 The vaporization of a liquid front moving slowly through a hot porous rock. Part II *J. Fluid Mech. in press*